Deliverable 4.12
Beryllium reactivity in magnesium phosphate cement

Date 28.6.2024 Version Final

Dissemination level Public

Sébastien Caes[1], Andrey Bukaemskiy[2], Guido Deissmann[2], Giuseppe Modolo[2], Valdir de Souza[1], Bruno Kursten[1]

1 SCK CEN, Boeretang 200, 2400 Mol, Belgium

2 Forschungszentrum Jülich GmbH, Wilhelm-Johnen-Straße, 52428 Jülich, Germany

sebastien.caes@sckcen.be; a.bukaemskiy@fz-juelich.de

This project has received funding from the Euratom research and training programme 2019-2020 under grant agreement No 945098.

Project acronym PREDIS	Project title PRE-DISposal management of radioactive waste	Grant agreement No. 945098
Deliverable No. D4.12	Deliverable title Beryllium reactivity in magnesium phosphate cement	Version Final
Type Report	Dissemination level Public	Due date M46
Lead beneficiary SCK CEN and Forschungszentrum Jülich GmbH		WP No. 4
Main authors Sebastien Caes, SCK CEN; Andrey Bukaemskiy, FZJ	Reviewed by Guido Deissmann, Giuseppe Modolo, FZJ; Valdir de Souza, Bruno Kursten, SCK CEN; Abdelouas Abdessalam, IMT, WP4 Leader	Accepted by Maria Oksa, VTT, Coordinator
Contributing authors FZJ: Guido Deissmann, Giuseppe Modolo; SCK CEN: Valdir de Souza, Bruno Kursten		Pages 50

Abstract

Due to its physical and mechanical properties, metallic beryllium is an attractive engineering material for nuclear applications, e.g. as moderator, reflector, or fuel cladding in thermal reactors. After use, activated beryllium waste will need to be disposed of in a geological disposal repository. One option for the treatment and conditioning of the beryllium waste could be the direct emplacement of pieces of beryllium in a cementitious matrix. In these conditions, beryllium corrodes producing hydrogen, and beryllium oxide and/or hydroxide. Different cement matrices could be used. The most common one is the Ordinary Portland Cement possessing a highly alkaline pore solution. However, other cementitious materials, such as the Magnesium Phosphate Cement possessing a near neutral pore solution can also be of interest. Indeed, because beryllium is an amphoteric material, decreasing the pH to more neutral conditions could be beneficial to decrease the corrosion rate.

In this study, the corrosion rate and mechanism of metallic beryllium is investigated in solutions mimicking the cement pore solutions as well as in different cementitious matrices using electrochemical impedance spectroscopy, the measurement of the hydrogen released, the mass loss, scanning electron microscopy and X-ray diffraction.

Coordinator contact

Maria Oksa
VTT Technical Research Centre of Finland Ltd
Kivimiehentie 3, Espoo / P.O. Box 1000, 02044 VTT, Finland
E-mail: maria.oksa.@vtt.fi
Tel: +358 50 5365 844

Acknowledgement

This project has received funding from the Euratom research and training programme 2019-2020 under grant agreement No 945098.

GLOSSARY OF ABBREVIATIONS

BR2	Belgian Reactor 2
BDID	Barrier Discharge Ionisation Detector
CR	Corrosion Rate
EEC	Equivalent Electrical Circuit
EIS	Electrochemical Impedance Spectroscopy
FZJ	Forschungszentrum Jülich
GC	Gas Chromatography
ICP-MS	Inductively Coupled Plasma – Mass Spectroscopy
LC-MPC	Low Cost Magnesium Phosphate Cement
ML	Mass Loss
MPC	Magnesium Phosphate Cement
MPC+B	Magnesium Phosphate Cement + Boric Acid
OPC	Ordinary Portland Cement
PP	Polypropylene
PSD	Continuous Position-Sensitive Detection
PVC	Polyvinylchloride
RPM	Revolutions Per Minute
SCK CEN	The Belgian Nuclear Research Centre
SEM-EDS	Scanning Electron Microscopy – Energy Dispersive X-Ray Spectroscopy
XRD	X-Ray Diffraction

TABLE OF CONTENTS

1 Introduction

Metallic beryllium has a high specific heat and thermal conductivity, and high specific strength and stiffness. Moreover, due to its low neutron-capture cross section and high potential for elastic neutron scattering, it is an attractive engineering material for nuclear applications, e.g. as moderator, reflector, or fuel cladding in thermal reactors. Inconveniences however are its toxicity in particulate form (leading to berylliosis and chronic beryllium disease), its low fracture toughness, and its high cost [1-3]. At SCK CEN, the beryllium waste originates from the matrix of the BR2 reactor composed of 79 cylindrical channels and contains fuel elements, control rods, experiment installations or reflector plugs made of beryllium [4]. Moreover, it is also under consideration as interesting material for future fusion power reactors (e.g., as first wall) [5-7].

One option for the treatment and conditioning of the beryllium waste could be the direct emplacement of pieces of beryllium in a cementitious matrix. The literature on the behaviour of beryllium in cementitious media is scarce [8, 9]. According to the thermodynamic data, beryllium is an amphoteric metal, which means that it is protected against corrosion in neutral to slightly alkaline media [10-12]. However, at high pH, beryllium is expected to corrode faster (up to a few µm/y) [9, 10], with the production of hydrogen gas under anaerobic conditions.

The use of cementitious matrices with a lower pore solution pH, e.g. Magnesium Phosphate Cement (MPC) could be an option to decrease the corrosion rate of beryllium and consequently, the hydrogen production, which could lead to build up of extra pressure in the geological disposal facility, and creating some stress problem (including potentially inducing stress on the host rock). Note that earlier literature [10, 13, 14] showed that the stability domain of beryllium was slightly shifted to higher pH (until a pH of 13.5, instead of ~12 as described by Pourbaix). Therefore, these new limits include the pH conditions encountered in ordinary Portland cement, commonly used for the encapsulation of nuclear wastes.

Therefore, within the frame of the collaborative EC-funded Horizon 2020 project PREDIS, the corrosion behaviour of beryllium was studied in MPC, as well as ordinary Portland cement (OPC), and in the representative cementitious pore solutions.

2 Experimental procedures

2.1 Materials

S-200-F grade beryllium pellets of ~3 mm thick and 15 mm in diameter (from BR2, 1980's campaign, SCK CEN) or beryllium foils (Alfa Aesar, 99.8% purity) with a thickness of 0.25 mm and dimension of 1.7 x 3.2 cm² were used as initial material. The beryllium foils were cleaned by rinsing them with acetone and ethanol and were treated with HCl (0.5 M) solution (around 1 min) as recommended in [14]. Then they were rinsed thoroughly with demineralized water and dried with a tissue paper. The beryllium pellets were initially cut from beryllium rods possessing a length of ~10 cm. After cutting, the pellets were washed with ethanol and milli-Q water.
To study the corrosion of beryllium samples by electrochemical techniques, working electrodes were produced by glueing a steel wire on the back side of a beryllium pellet using CW2400 conductive adhesive (Chemtronics). After hardening of the adhesive, a heat-shrunk Teflon® tube was slipped over the steel wire to avoid contact with the test media. Finally, the metallic pellet/steel wire was placed inside a PVC ring and an epoxy resin was poured to insulate completely the connection from the external media. Prior to each electrochemical test, the beryllium electrode was polished to a P1200 SiC emery paper finish using a Minimet 1000 polishing machine (Buehler). Directly after being polished, the electrodes were transferred into a glovebox under argon atmosphere to avoid as much as possible the oxidation of the polished surface[1].

Beryllium corrosion tests were done in solution representative of ordinary Portland cement pore water (OPC solution), in solution representative of magnesium phosphate cement pore water (MPC solution), and in simple NaOH solutions. Different cement paste/mortars were also used: OPC, MPC[2] and low cost magnesium phosphate cement (LC-MPC[3]). The composition of these solutions and cement pastes/mortars are given in Table 1 and Table 2, respectively. Note that boric acid was added neither to the solutions nor to the mortars at SCK CEN.

Table 1. Composition of the solutions used for the corrosion study of beryllium.

Solutions	Composition	Na^+	K^+	SO_4^{2-}	PO_4^{3-}	H_3BO_3	pH
OPC solution	mol/L	0.14	0.37	2×10^{-3}	-	-	13.5
	g/L	3.22	14.47	0.19	-	-	
MPC solution	mol/L	-	3.76	-	1.98	0 – 0.54	7.7 – 8.1
	g/L	-	150.40	-	188.05	0 – 33.39	
NaOH solutions*	mol/L	$1x10^{-7}$ – 0.89	-	-	-	-	6.7 – 14.0
	g/L	$2x10^{-6}$ – 20.47	-	-	-	-	

** NaOH solution at pH 6.7 could be obtained from ultra-pure water possessing an initial pH around 6.0.*

[1] The polishing step might not be done directly in the glove box under argon atmosphere to avoid contamination with toxic beryllium dust.
[2] Use of hardburnt MgO (MAGCHEM 10CR) from Martin Marietta Magnesia Specialties.
[3] Use of reactive MgO (AK98VHR) from Timab.

Table 2. Formulation for 1L of cement paste/mortars used for the corrosion study of beryllium.

Cement paste/mortars	CEM I 52.5N	MgO	KH_2PO_4	Quartz sand	Fly Ashes	H_3BO_3	$Na_2S_2O_3 \cdot 5H_2O$	H_2O
OPC (g)	1600	-	-	-	-	-	-	800
MPC (g)	-	131.39	443.58	574.97	574.97	0 – 11.5	-	293.24
LC-MPC (g)	-	128.72	437.13	565.86	565.86	-	28.30	288.59

For the tests carried out at SCK CEN, in order to limit as much as possible the quantity of oxygen in the system to mimic the deep geological conditions, OPC and MPC solutions and cement pastes/mortars were produced in a glove box under argon atmosphere (less than 1 µL/L O_2 in the gas phase; less than 1 nL/L O_2 in solution)[4]. Except for the preparation of LC-MPC, which followed the procedure reported in [15], the mixtures (dry powders and milli-Q water) were stirred manually for 10 minutes.

2.2 Corrosion tests

Four types of corrosion tests were performed: (i) mass loss (ML) tests, (ii) Inductively Coupled Plasma – Mass Spectroscopy (ICP-MS) tests, (iii) hydrogen measurement tests and (iv) electrochemical tests. While the mass loss and ICP-MS tests were only performed with beryllium samples immersed in solution, hydrogen measurement tests and electrochemical tests were realised on beryllium samples immersed in solution and on beryllium samples embedded in cementitious matrices.

2.2.1 Mass loss and ICP-MS tests

The corrosion experiments were carried out in tightly sealed plastic containers with a volume of 500 mL under air atmosphere.
Beryllium corrosion tests were performed in different solutions representative of Ordinary Portland Cement pore water (OPC solution, pH = 13.43), magnesium phosphate cement pore water (MPC solution, pH = 7.91) and magnesium phosphate cement pore water with the addition of boric acid (MPC+B solution, pH = 7.73). Moreover, five model NaOH solutions with pH values equal to 6.71, 12.54, 13.26, 13.42 and 13.99 were used. Special studies were conducted to determine the accuracy of the pH measurements; for all solutions used, the measurement error did not exceed 0.02 pH units. The initial volume of all solutions was 250 mL. The total duration of the corrosion experiments for beryllium was 120 days for OPC, MPC, MPC + B and NaOH (pH = 6.71 and 13.42) solutions. For the NaOH solutions with pH equal to 12.54, 13.26 and 13.99 the total duration of the corrosion experiments was 30 days. The sampling periodicity was once every 1-3 days. The beryllium samples were removed from the solution, thoroughly washed with demineralized water, carefully dried with a soft tissue paper following the procedure recommended by Bouhier *et al.* [14] and weighed. To increase the measurement accuracy and determine the measurement error, each sample was weighed five times.

[4] LC-MPC was not prepared in a glove box under argon atmosphere to avoid disturbing other running electrochemical tests, due to the vibration produce during the harsher stirring procedure (up to 1200 rotations per minute).

In addition, 2 mL of the leaching solution was abstracted for subsequent determination of beryllium concentrations by using ICP-MS (Elan 6100 DRC). After sampling, the solution was not supplemented; the change in solution volume was taken into account in the calculation of the corrosion rates.

2.2.2 Hydrogen measurement tests

Hydrogen measurement tests consist of measuring the hydrogen gas formed during the corrosion of beryllium in aqueous solutions in anaerobic argon atmosphere. The oxidation of beryllium depends on the pH as shown by Cannes *et al.* [10]. Therefore, at pH close to 8 up to 10.5 (as observed in MPC and in the MPC solution), the oxidation of beryllium is given by Equation 1:

$$Be + 2H_2O \rightarrow Be(OH)_2 + H_2 \qquad \text{(Equation 1)}$$

At higher pH, the oxidation of beryllium is given by Equation 2 and Equation 3:

$$Be + OH^- + 2H_2O \rightarrow Be(OH)_3^- + H_2 \qquad \text{(Equation 2)}$$

$$Be + 2OH^- + 2H_2O \rightarrow Be(OH)_4^{2-} + H_2 \qquad \text{(Equation 3)}$$

However, for all pH's, when one mole of beryllium is oxidised, one mole of dihydrogen is formed. Therefore, by measuring the volume of hydrogen produced in function of time, the corrosion rate can be established using the same calculation in all conditions (all pH).

These tests were carried out under anaerobic argon atmosphere in 1 L leak-tight steel containers coated with a Teflon® liner to avoid the corrosion of steel. The hydrogen gas concentration inside the container was measured by a Shimadzu GC-2010 Plus type gas chromatograph (GC) equipment, using a ShinCarbon ST column and a Barrier Discharge Ionisation Detector (BDID), on a regular basis. The H_2 concentration was quantified by comparing the area under the H_2 peak with a calibration curve performed by injecting argon gas containing 1 to 10000 µL/L H_2. Before and after the sample measurements, a 100 µL/L H_2/Ar gas was injected in the GC for quality control. Because the container volume is known, the amount of hydrogen generation over a given time interval can be determined and correlated to the corrosion rate of beryllium. To lower as much as possible the volume of H_2 gas adsorbed on the wall of the container or trapped in the cement paste, the containers were slightly shaken for several times before sampling. The atmosphere in the container was thoroughly refreshed by argon after each measurement to remove the residual hydrogen generated during the previous period. As an example, one calculation is presented in Annex 1.

2.2.2.1 Tests in representative cement paste pore solutions

Three beryllium pellets were placed in each container to get a sufficient surface area in contact with the solution. This also increases the volume of hydrogen formed, leading to an easier measurement by the GC. Each test was done in triplicate to ensure the reproducibility of the tests.

2.2.2.2 Tests in cement pastes

These tests were done with samples embedded in cement pastes in different steps: (1) three cement paste/beryllium samples were placed in a container above water (to get a 100% relative humidity atmosphere) to allow a controlled curing of the cement paste in the first days of the tests; (2) after 28 days, the underlying water was removed and the test was continued for ~6 weeks in dry

conditions; (3) the corresponding solution representative of the cement pore water was injected in the container to immerse completely the samples. This step allowed to study the re-initiation of corrosion after water re-saturation of the cement paste, mimicking water infiltration after potential breach of the envelope of the waste container. Note that in these tests, the porous network is not supposed to dry completely after only 6 weeks in dry conditions.

2.2.3 Electrochemical tests

Electrochemical cells consisted of a working electrode (the beryllium electrode), a counter electrode (Inconel 625, which was previously passivated in the corresponding electrolyte for a minimum of two weeks) and a reference electrode (Ag/AgCl in KCl 0.1 M). When the electrodes were embedded in the cement pastes, no Ag/AgCl electrode was embedded in the cementitious matrix. Therefore, the reference electrode and the counter electrode were connected together to the Inconel 625 plate to have a two electrode system. The two electrodes were positioned 5 mm apart using PVC spacers. All electrodes were connected to an Autolab PGSTAT 302F potentiostat (Metrohm) combined with the NOVA 1.8 version software.

Three different system configurations were studied:

- First, the electrochemical behaviour of metallic beryllium was analysed by Electrochemical Impedance Spectroscopy (EIS) while immersed in OPC or MPC solutions (see Section 2.1 for the composition of the solutions).
- Second, the electrochemical behaviour of beryllium metal in contact with the OPC paste or MPC mortar was analysed by immersing the electrodes in a vial filled with cement paste/mortar.
- Third, to study the effect of the re-initiation of corrosion after water re-saturation of the cement paste, hardened[5] cement pastes/mortars containing the electrodes were immersed in OPC or MPC pore water solution.

EIS spectra were recorded at the open circuit potential (OCP) with a 10 mV amplitude. The frequency ranged between 10^5 Hz to 10^{-2} Hz, with 10 frequency values per logarithmic decade. The analysis and the fit of the spectra were performed using the software 'Zview'. All tests were done in triplicate to evaluate the reproducibility.

Depending on the test, different equivalent electrical circuits (EEC) where used to fit the EIS curves. Figure 1 shows all EEC used during the corrosion of beryllium. For tests performed in OPC solution, the EEC represented in Figure 1a was used. This EEC possess two R//C circuit in parallel, where the pure capacitors are replaced by constant phase elements to take into account the heterogeneity of the electrolyte/metal interface [10]. The circuit R1//CPE1 is used to model the oxide layer formed at the surface of the beryllium. CPE_{dl} is used to model the double layer capacitance and R_t is used to model the charge transfer resistance. Note that because of the high conductivity of the electrolyte used (not measured), the resistance of the electrolyte was negligible and therefore it was not taken into consideration is the EEC circuit. For tests in MPC solution, the EEC described in Figure 1b was used. This EEC is composed of a resistance of the electrolyte[6] (R_s), a circuit $R_l//L_l$ used to model the induction loop observed at high frequency in the Nyquist plots, a constant phase element CPE_{dl} to model the double layer capacitance and R_t to model the charge transfer resistance. Figure 1c shows

[5] Hardened in glove box under argon atmosphere for 1 day before immersion in solution.
[6] Even if the conductivity of the MPC solution is also high, the fit was better when R_s was added to the EEC.

the EEC used to fit the data recorded for beryllium embedded in OPC paste. The first part of the EEC is composed of three branches in parallel corresponding to the electrochemical properties of the cement paste between two electrodes, as described elsewhere [16, 17]. The second part corresponds to the electrochemical response of the beryllium/cement paste interfaces. Finally, Figure 1d shows the EEC used to fit the data recorded for beryllium embedded in OPC paste. This EEC is similar to the one used for the tests done in OPC, except that an extra R//C branch is added to fit the electrochemical properties of the cement paste, as explained by [13, 14]. Note that R_t is the most important parameter for this study, as it is used to calculate the corrosion rate of beryllium, as explained below.

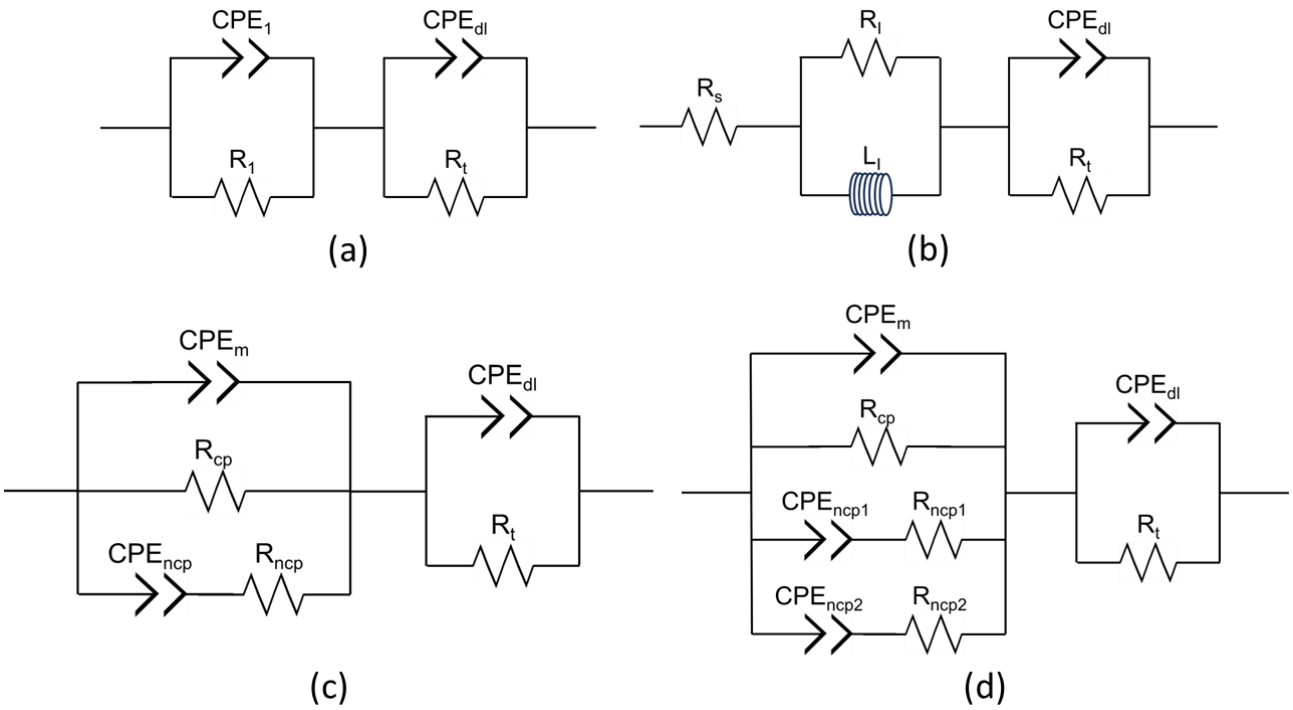

Figure 1. Equivalent electrical circuits used to fit the EIS curves. (a) EEC used to fit tests performed in OPC solution. (b) EEC used to fit tests performed in MPC solution. (c) EEC used to fit tests performed in OPC and OPC immersed in OPC solution. (d) EEC used to fit tests performed in (LC-)MPC and in (LC-)MPC immersed in MPC solution.

The fitting of EIS spectra provides the values of the charge transfer resistance (R_t) in the corrosion process. Using this value, the corrosion current, I_{corr} (A), is calculated by Equation 4, as described in [13]:

$$I_{corr} = \frac{RT}{n_c \alpha_c \mathcal{F} R_t}, \qquad \text{(Equation 4)}$$

where R is the gas constant (J/(K·mol)), T is the temperature (K), n_c is the number of electron involved (2 for the oxidation of beryllium), α_c is the charge transfer coefficient (approximated at 0.5), $\mathcal{F}$ is the Faraday constant (C) and R_t is the charge transfer resistance (Ω).

The corrosion current density, i_{corr} (A/cm²), is given by Equation 5:

$$i_{corr} = \frac{I_{corr}}{S}, \quad \text{(Equation 5)}$$

where S is the exposed surface of the electrode (cm²).

The corrosion rate (v_{corr} *in µm/y*) is then calculated using Equation 6:

$$\upsilon_{\mathrm{corr}} = 3.27 \times 10^{6} \times \frac{\mathrm{i_{corr}}}{\rho} \times \mathrm{EW}\ , \quad \text{(Equation 6)}$$

where ρ is the metal density (g/cm³, ρ_{Be} = 1.85 g/cm³) and *EW* is the equivalent weight. *EW* is calculated by dividing the atomic weight of an element by the valence of the metal, hence, for beryllium the atomic weight is 9 and the valence is 2, so EW_{Be} = 4.5.

2.3 Characterisation techniques

2.3.1 Scanning Electron Microscopy – Energy Dispersive X-ray Spectroscopy (SEM-EDS)

SEM-EDS characterisation of the surface of the beryllium samples or the cross section of embedded samples was carried out with a Phenom apparatus (SEM, Phenom PRO X, Thermo Fisher Scientific, The Netherlands) using an accelerating voltage of either 10 kV or 15 kV. As there is no internal standard in the apparatus, EDS only provides semi-quantitative analysis and percentage below 1 at.% are not taken into account. Moreover, no information on beryllium can be recorded because this element is too light and cannot be detected by the EDS detector.

2.3.2 X-Ray Diffraction (XRD)

XRD measurements were performed to analyse the crystal phases present at the surface of the beryllium samples corroded in solution. The measurements were done with a Bruker©D8 Advance diffractometer operating in Bragg- Brentano configuration and using a Cu-LFF X-ray tube (Cu $K_{\alpha 1}$ = 0.15405929 nm) at 40 mA and 40 kV. Diffracted X-rays were detected by a position-sensitive real time multiple strip detector (Lynxeye) operated in the continuous position-sensitive detection (PSD) mode, with a PSD opening of 3.3°(2 θ). The incident beam was collimated by a variable divergence slit set to an illumination length of 15 mm, and axial Soller slits of 2.5°. The diffracted beam passed through axial Soller slits of 2.5° and a Ni filter. The beryllium samples were mounted onto a rotating sample stage and diffractograms were recorded while applying a rotation speed of 15 rotations/min. Diffractogram acquisitions were performed by scanning from 5°- 90° with a step size of 0.02° (2 θ). The X-ray diffractograms were evaluated with HighScore Plus software (v4.9).

2.3.3 Inductively Coupled Plasma Mass Spectrometry (ICP-MS)

ICP-MS measurements were performed to analyse the beryllium concentration in solution at the end of the tests performed in solution. The measurements were done with a XSERIES2 apparatus (Thermo Scientific, USA) on samples diluted and acidified with 1 % HNO_3. The detection limit for beryllium is <1 µg/kg.

3 Results and Discussion

3.1 Corrosion tests in solutions

3.1.1 Electrochemical measurement (Electrochemical Impedance Spectroscopy)

3.1.1.1 Evolution of the Nyquist and Bode diagrams[7]

The evolution of the Nyquist and Bode diagrams of beryllium immersed in OPC solution in function of time is shown in Figure 2 and the fitting values are given in Table 3 using the EEC described in Figure 1a. The Nyquist plots (Figure 2 (a and b)) are represented by two semi-circles. The one at high frequency corresponds to the impedance of the oxide layer present at the surface of the metal and it does not evolve significantly with time (until 135 days of test). However, at lower frequency, the second semi-circle diameter increased with time (from ~8000 to ~22000 Ω), revealing a decrease of the corrosion rate with time. For few tests, some induction could be observed at high frequency (loop going below the x-axis in Figure 2b), but this is supposed to be related to the electrical wires used to connect the studied system to the potentiostat, rather than to the corrosion process. For these tests, a R//I circuit in parallel was added in series to the EEC of Figure 1a. The Bode plots also revealed the increase of the impedance modulus with time at low frequencies (Figure 2c), while the phase angle remained the same during the entire period of time (Figure 2d).

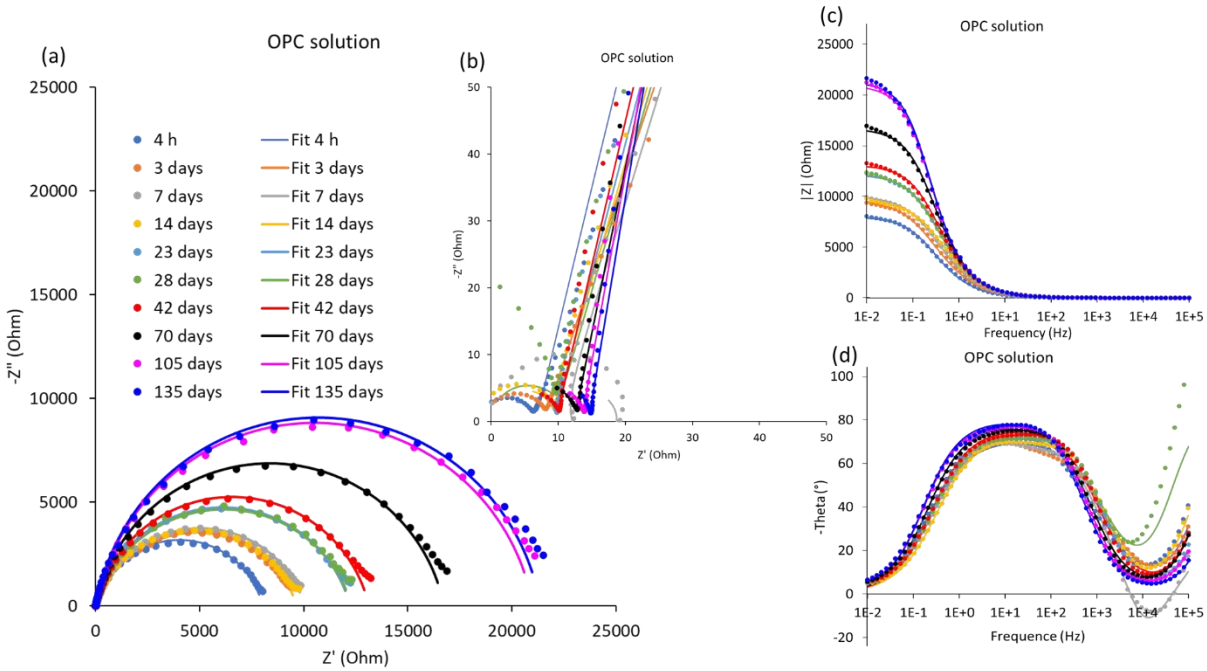

Figure 2. (a and b) Evolution of the Nyquist spectra and (c and d) evolution of the Bode spectra of beryllium in OPC solution in function of time (dots: experimental results; lines: fit).

[7] Note that these information represent only one of the triplicate. However, tests were reproducible and the corrosion rate (see Section 3.1.2.2) was calculated using the average value of R_t.

Table 3. Fitting data of the EIS spectra of beryllium in OPC solution.

Days	R_1 (Ω)	CPE_1		CPE_{dl}		R_t (Ω)
		K_1 ($F \cdot S^{\alpha}$)	α_1	K_{dl} ($F \cdot S^{\alpha}$)	α_{dl}	
1	6.7	9.3×10^{-7}	0.89	9.7×10^{-5}	0.86	8010
3	8.0	1.6×10^{-7}	0.97	8.1×10^{-5}	0.80	9700
7*	10.1	9.6×10^{-8}	1	6.7×10^{-5}	0.82	10040
14	9.1	1.2×10^{-7}	1	5.8×10^{-5}	0.83	9650
23	9.3	5.8×10^{-8}	1	5.3×10^{-5}	0.84	12210
28	9.5	4.0×10^{-7}	1	5.5×10^{-5}	0.82	12300
42	9.7	8.2×10^{-8}	1	5.0×10^{-5}	0.86	13130
70	12.4	6.4×10^{-8}	1	4.7×10^{-5}	0.88	16720
105	13.5	4.1×10^{-8}	1	4.5×10^{-5}	0.89	21000
135	14.5	2.8×10^{-8}	1	4.5×10^{-5}	0.90	21340

*Presence of induction in the Nyquist plot. Therefore, a R_l//L_l circuit was added in series to the circuit described in Figure 1a. The value of R_l equals 10.2 Ω. The value of L_l equals 1.1×10^{-4} Henry.

The evolution of the Nyquist and Bode diagrams of beryllium immersed in MPC solution in function of time was also recorded (Figure 3) and the fitting values, obtained using the EEC described in Figure 1b, are shown in Table 4. The Nyquist plots are composed of an inductive loop at high frequencies (Figure 3b), followed by one semi-circle at medium to low frequencies (Figure 3a). Note that another semi-circle seems to appear in the low frequency region (especially at the beginning of the test) (Figure 3a). However, measurements at lower frequencies would have been needed to be able to interpret this phenomenon.

At high frequencies, all measurements were similar until 50 days (Figure 3b), with the presence of an inductive loop and a low R_s value between 2 and 11 Ω. However, after 50 days, the R_s value increased to 165 to 212 Ω. A modification in phase evolution in the Bode diagram was also observed as the peak moved to lower frequencies (Figure 3d).

Contrary to the tests done in OPC solution, Figure 3a shows that the diameter of the semi-circle decreased with time until it reached values close to 8000 Ω, revealing a first increase of the corrosion rate before a stabilisation at a higher rate.

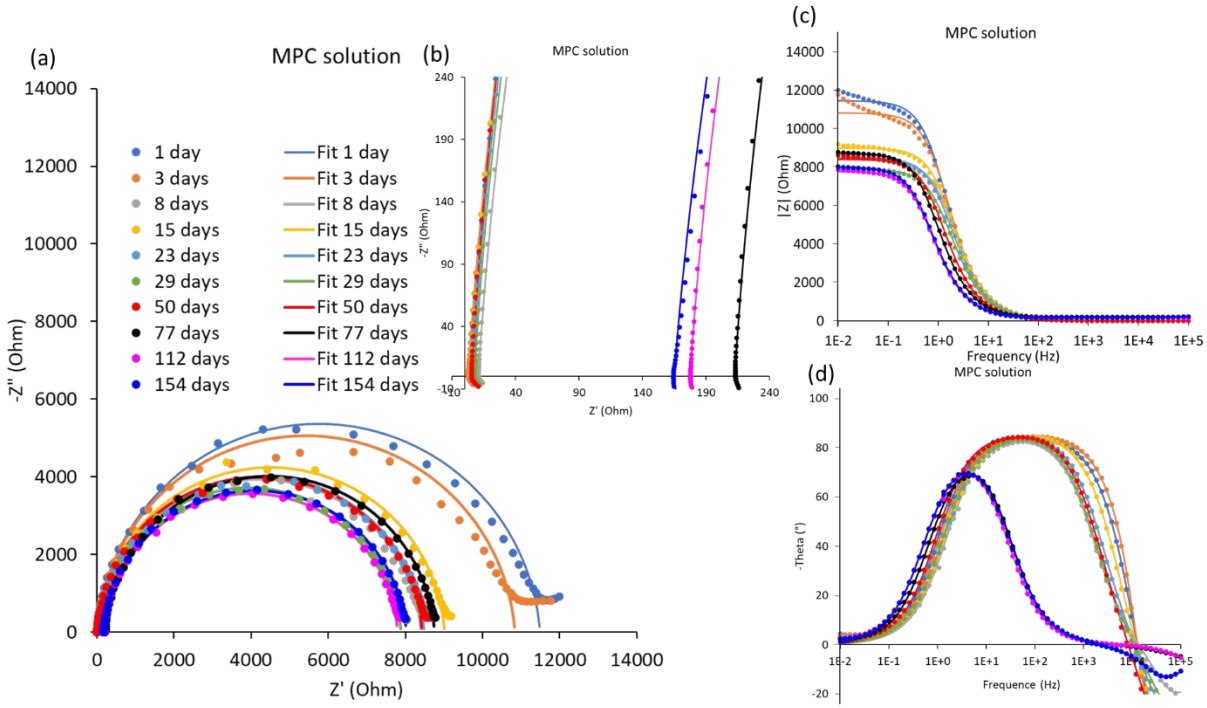

Figure 3. (a and b) Evolution of the Nyquist spectra and (c and d) evolution of the Bode spectra of beryllium in MPC solution in function of time (dots: experimental results; lines: fit).

Table 4. Fitting data of the EIS spectra of beryllium in MPC solution.

Days	R_s (Ω)	R_l (Ω)	L_l (Henry)	CPE_{dl}		R_t (Ω)
				K_{dl} ($F \cdot S^{\alpha}$)	α_{dl}	
1	3.0	13.8	1.7×10^{-5}	1.5×10^{-5}	0.96	11480
3	2.4	14.6	1.8×10^{-5}	1.4×10^{-5}	0.96	10830
7	10.5	11.2	1.6×10^{-5}	1.4×10^{-5}	0.96	8390
15	4.4	11.5	2.0×10^{-5}	1.4×10^{-5}	0.96	9000
23	6.3	11.0	2.0×10^{-5}	1.6×10^{-5}	0.96	8470
29	7.6	12.9	1.8×10^{-5}	1.7×10^{-5}	0.96	7870
50	5.0	16.1	2.4×10^{-5}	2.2×10^{-5}	0.97	8430
77	212.4	36.4	4.7×10^{-5}	2.9×10^{-5}	0.96	8530
112	177.3	61.8	2.9×10^{-5}	4.1×10^{-5}	0.96	7620
154	164.9	96.7	2.4×10^{-5}	4.0×10^{-5}	0.95	7870

3.1.1.2 Corrosion rate calculation

Once R_t has been obtained via the fitting of the EIS data, the corrosion rate of beryllium was calculated using Equations 4 to 6. The evolution of the corrosion rate with time is shown in Figure 4 and Table 5. Initially, the corrosion rate of beryllium was lower in MPC solution (pH 8.1) than in OPC solution (pH 13.5). However, the corrosion rate in OPC solution decreased with time, while it increased before to stabilise at ~15 µm/y in MPC solution. Therefore, after 7 days, the corrosion rate became lower in OPC solution than in MPC solution. At the end of the test (4-5 months), the corrosion of beryllium was three times lower in OPC solution (high pH) than in MPC solution (near neutral pH). Cannes *et al.* [10] also analysed the corrosion of beryllium in different pH solutions composed of HCl

and NaOH and the charge transfer resistance at pH ~8 was also lower (and therefore the corrosion rate higher) than the one expected at pH 13.5 (only measured at pH 13 and 14 in [10]).

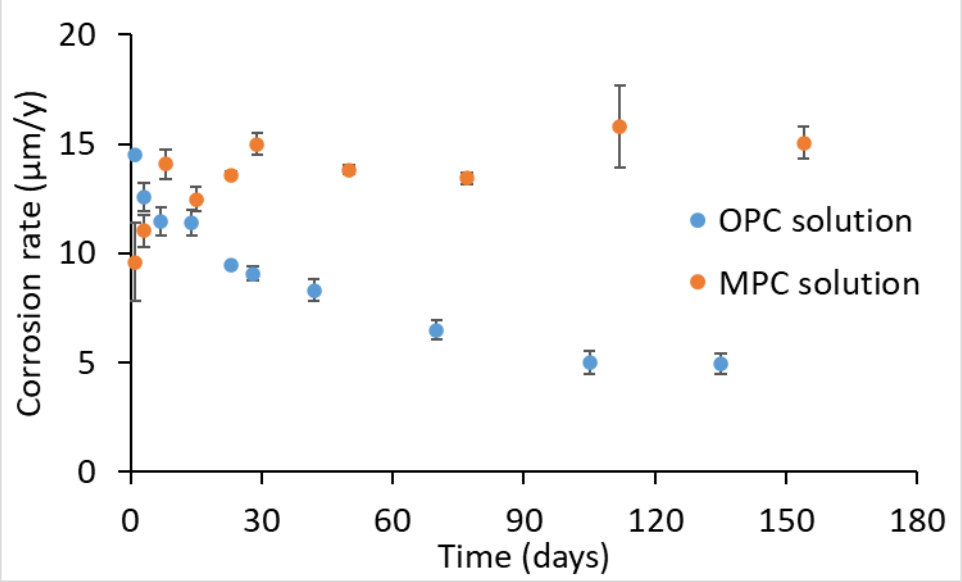

Figure 4. Evolution of the corrosion rate of beryllium with time in OPC and MPC solutions.

Table 5. Average charge transfer resistance and corrosion rate and of beryllium in OPC and MPC solutions.

OPC solution			MPC solution		
Days	R_t (Ω)	Corrosion rate (µm/y)	Days	R_t (Ω)	Corrosion rate (µm/y)
1	7970 ± 80	14.5 ± 0.1	1	12040 ± 1190	9.6 ± 1.8
3	9190 ± 1410	12.6 ± 0.7	3	10480 ± 350	11.0 ± 0.7
7	10110 ± 680	11.4 ± 0.7	8	8210 ± 190	14.1 ± 0.7
14	10140 ± 1520	11.4 ± 0.6	15	9270 ± 200	12.5 ± 0.5
23	12200 ± 20	9.5 ± 0.01	23	8520 ± 50	13.6 ± 0.1
28	12750 ± 500	9.1 ± 0.3	29	7710 ± 130	15.0 ± 0.5
42	13910 ± 2290	8.3 ± 0.5	50	8360 ± 70	13.8 ± 0.2
70	17830 ± 3260	6.5 ± 0.4	77	8610 ± 90	13.4 ± 0.3
105	23130 ± 6090	5.0 ± 0.5	112	7320 ± 420	15.8 ± 1.9
135	23420 ± 4940	4.9 ± 0.5	154	7680 ± 190	15.1 ± 0.7

3.1.2 Hydrogen measurement test

3.1.2.1 Hydrogen production and corrosion rate calculation

The evolution of the hydrogen gas released during the corrosion of beryllium in OPC and MPC solutions was measured during one year (Figure 5 and Table 6).
In OPC solution, the initial corrosion rate (after 7 days in solution) was slightly lower than 7 µm/y, which corresponds to a release of 84 mL $H_2/m^2 \cdot d$. This rate decreased with time until reaching a plateau at 1.8 µm/y and 23 mL $H_2/m^2 \cdot d$ produced after 240 days. Because the surface area of beryllium in contact with the solution was known (assuming a flat surface), it was also possible to calculate the thickness of corroded beryllium, based on the hydrogen formed during the test. Table 6 shows that after one year, around 3.2 µm of beryllium was corroded in OPC solution.

In MPC solution, the corrosion rate was initially higher and remained constant at around 12 µm/y (~150 mL $H_2/m^2 \cdot d$) during the first 180 days. At that time, a sudden decrease of the corrosion rate/hydrogen release was observed until an extremely low corrosion rate around 0.2 µm/y (2.5 mL $H_2/m^2 \cdot d$). This sudden decrease of the corrosion rate of beryllium in MPC solution could be due to the formation of a protective layer at the surface of the metal. The thickness of corroded beryllium was also calculated to ~6.6 µm, based on the hydrogen formed during the test in MPC solution.

Interestingly, the corrosion rates calculated from the generation of hydrogen are in good agreement with the ones obtained by EIS. Unfortunately, the EIS tests only lasted 154 days in MPC solution. Therefore, the decrease of the corrosion rate observed during the hydrogen measurement test could not be confirmed by EIS.

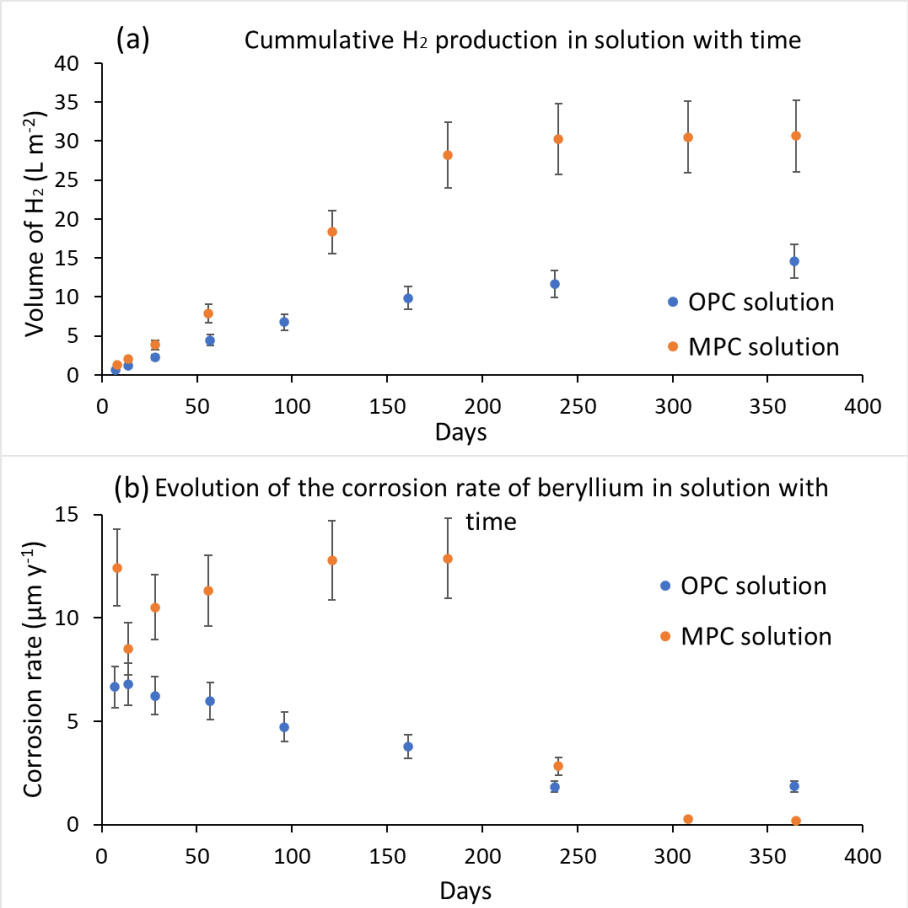

Figure 5. Leaching tests of beryllium pellets in OPC and MPC solutions. (a) Evolution of the cumulative volume of hydrogen produced with time and (b) Evolution of the corresponding corrosion rate with time.

Table 6. Volume of hydrogen released, corresponding corrosion rate and calculated thickness of corroded beryllium in OPC and MPC solutions.

OPC solution					MPC solution				
Days	Cumulative VH_2 production (L/m^2)	VH_2 between two sampling ($L/m^2 \cdot d$)	Calculated corrosion rate (µm/y)	Cumulative thickness of corroded Be (µm)	Days	Cumulative VH_2 production (L/m^2)	VH_2 between two sampling ($L/m^2 \cdot d$)	Calculated corrosion rate (µm/y)	Cumulative thickness of corroded Be (µm)
7	0.6	8.4×10^{-2}	6.7	0.13	8	1.2	1.6×10^{-1}	12.4	0.27
14	1.2	8.6×10^{-2}	6.8	0.26	14	2.0	1.1×10^{-1}	8.5	0.41
28	2.3	7.9×10^{-2}	6.2	0.50	28	3.9	1.3×10^{-1}	10.5	0.82
57	4.5	7.5×10^{-2}	6.0	0.97	56	7.9	1.4×10^{-1}	11.3	1.68
96	6.8	6.0×10^{-2}	4.7	1.47	121	18.3	1.6×10^{-1}	12.8	3.96
161	9.9	4.8×10^{-2}	3.8	2.15	182	28.2	1.6×10^{-1}	12.9	6.11
238	11.7	2.3×10^{-2}	1.8	2.53	240	30.3	3.6×10^{-2}	2.8	6.56
-	-	-	-	-	308	30.5	3.6×10^{-3}	0.3	6.61
364	14.6	2.3×10^{-2}	1.8	3.17	365	30.7	2.4×10^{-3}	0.2	6.64

3.1.2.2 Characterisation of samples from H_2 measurement tests

At the end of the hydrogen formation measurement tests, the OPC and MPC solutions were collected for analysis by ICP-MS. The concentrations of beryllium ions after one year of testing are given in Table 7.

Table 7. Beryllium concentration measured by ICP-MS in OPC and MPC solutions after one year of corrosion.

	OPC solution				MPC solution			
	Test 1	Test 2	Test 3	Average	Test 1	Test 2	Test 3	Average
[Be] (mg/L)	11.4±0.9	11.1±0.9	11.1±0.9	11.2±1.6	13.1±2.4	15.5±2.5	11.6±2.3	13.4±4.1
[Be] (mol/L)	(1.26±0.10) $\times10^{-3}$	(1.23±0.10) $\times10^{-3}$	(1.23±0.10) $\times10^{-3}$	(1.24±0.18) $\times10^{-3}$	(1.45±0.27) $\times10^{-3}$	(1.72±0.28) $\times10^{-3}$	(1.29±0.26) $\times10^{-3}$	(1.49±0.46) $\times10^{-3}$
Be surface area (cm^2)	15.47±0.02	15.48±0.07	15.67±0.07	15.54±0.10	15.88±0.03	15.57±0.05	15.41±0.02	15.62±0.06
Average Corrosion depth after 1 year (µm)	2.79±0.28	2.71±0.27	2.68±0.27	2.73±0.47	2.60±0.26	3.09±0.31	2.28±0.23	2.66±0.49

Because the surface area of beryllium in contact with the solution is known (assuming a flat surface), it was also possible to calculate the thickness of corroded beryllium based on the concentration of beryllium in solution. In OPC solution, a layer of about 2.73 µm thick would have been corroded after one year. This value is similar to the one calculated from the measurement of hydrogen release (3.17 µm; Table 6). This reveals that most of the oxidised beryllium should be released in solution and that the corrosion product layer at the surface of the metallic beryllium should be thin and non-protective. Cannes *et al.* [10] showed in a solubility diagram that for beryllium concentration ~1×10^{-3} mol/L in solution at pH 13.5, the system should be in the passive region in the $Be(OH)_{2\alpha}$ domain. However, these conditions are close to the border between $Be(OH)_2$ domain (passive region) and $Be(OH)_4^{2-}$ domain (active corrosion region).

The same calculation was done for tests performed in MPC solution: a layer of about 2.66 µm thick would have been corroded after one year. This value is lower than the one calculated from the measurement of hydrogen release (6.64 µm; Table 6). This could be caused by the lower solubility of beryllium in near neutral solution. Indeed, Çevirim-Papaioannou et al. [11, 18] showed that the beryllium solubility in NaCl, KCl or $CaCl_2$ at pH 8 could be as low as 10^{-5}-10^{-6} mol/L. Moreover, some

crystals were observed at the bottom of the test containers and the surface of the berylllium samples was darker, assuming precipitation of beryllium.

To gain more information on the surface and the cross section of the corroded beryllium pellet, as well as on the precipitates observed at the end of the tests in MPC solution, SEM-EDS (Figure 6 to Figure 11) and XRD analyses were carried out (Figure 12).

Figure 6 shows the initial surface of the S-200-F grade beryllium pellets, prior to testing. Straight scratches were present on the surface of the sample due to the sawing process used to produce the pellets. Some white particles were also visible, and an EDS analysis (not shown) revealed the presence of Fe, C, Si and Al in these particles, which are impurity elements present in the S-200-F grade beryllium.

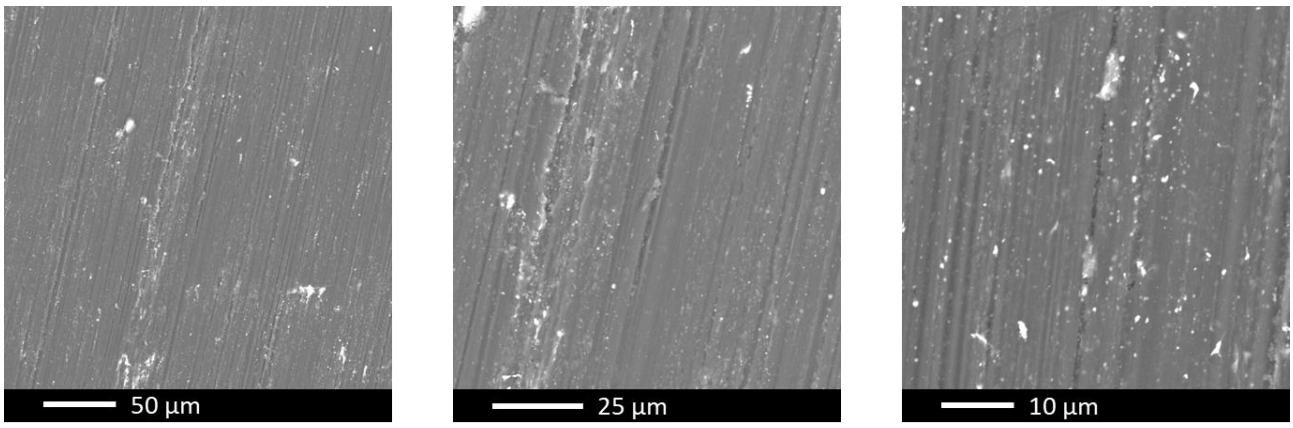

Figure 6. SEM micrographs of the surface of the initial beryllium samples prior to testing.

After one year in OPC solution (Figure 7), even if the scratches initially present were still visible, the surface of the beryllium samples was corroded. The whole surface consisted of a crater-like structure due to the presence of pits of 1 to 2 µm in diameter. However, many of these pits coalesced resulting in an increased size until a few tens of micrometres. From the pictures of the cross section (Figure 8), the pits were also visible, revealing a maximum depth of ~25 µm. The cross section also showed that there was no or thin corrosion product layer at the surface of the beryllium, confirming that beryllium, when oxidised, was mainly released in solution.

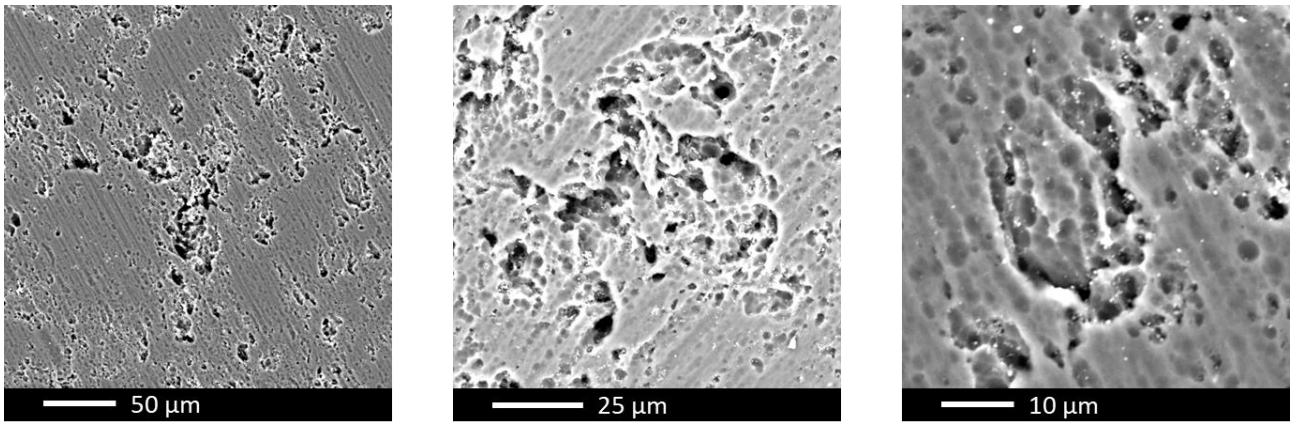

Figure 7. SEM micrographs of the surface of the beryllium samples corroded in OPC solution for one year.

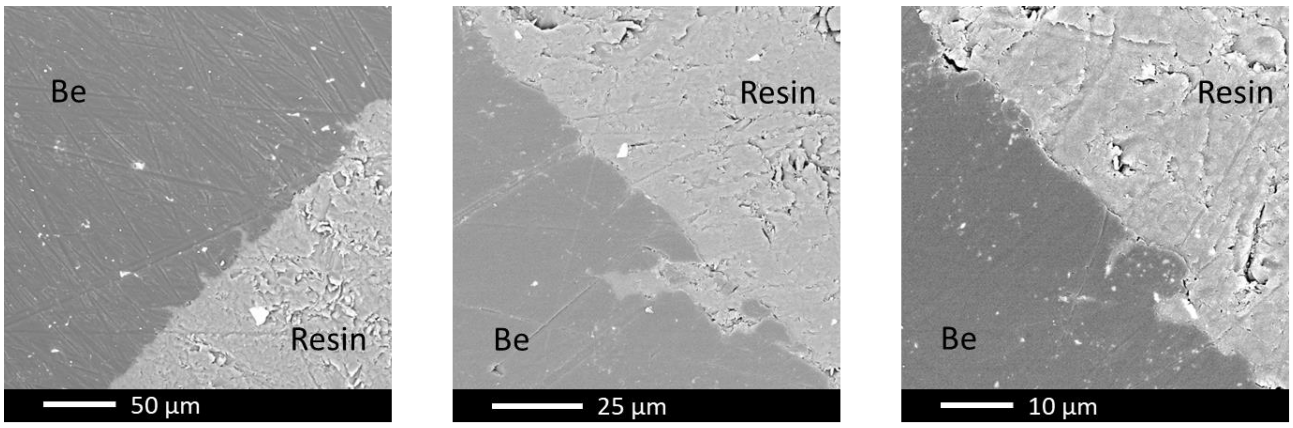

Figure 8. SEM micrographs of the cross section of the beryllium corroded in OPC solution for one year.

Contrary to the beryllium samples corroded in OPC solution, the surface of the beryllium samples corroded for one year in MPC solution was covered by needle-like crystals with a length going from a few hundreds of nanometres up to ~30 µm long (Figure 9). Sometimes, these crystals were found to be organised in a spherical shape. Cross section analyses (Figure 10) confirmed the presence of these spherical shaped crystals (Figure 10(a-c)), as well as needle-shaped crystals randomly covering the surface of the sample. Cross section analysis also revealed the presence of a corrosion product layer between the beryllium metal and the crystal layer having a thickness ranging from 5 to 20 µm.
Even if the detection of beryllium was not possible by EDS, point analyses revealed that the crystals were only composed of K, P and O (and Be; see XRD patterns below), while the corrosion product layer also contained element such as Ca and Mg (Table 8). Therefore, the corrosion product layer contains elements present as impurities in the beryllium metal, while the crystals consisted of elements only coming from the MPC solution (and beryllium).

The presence of these crystal layers could be the reason of the sudden decrease of the corrosion rate measured during the hydrogen measurement test after 180 days, as it could hinder the access of water to the surface of the beryllium, once these crystals covered the entire surface of the metallic samples. This hypothesis could also suggest that the crystals are formed in a later stage, maybe once the beryllium concentration in MPC solution reach saturation.

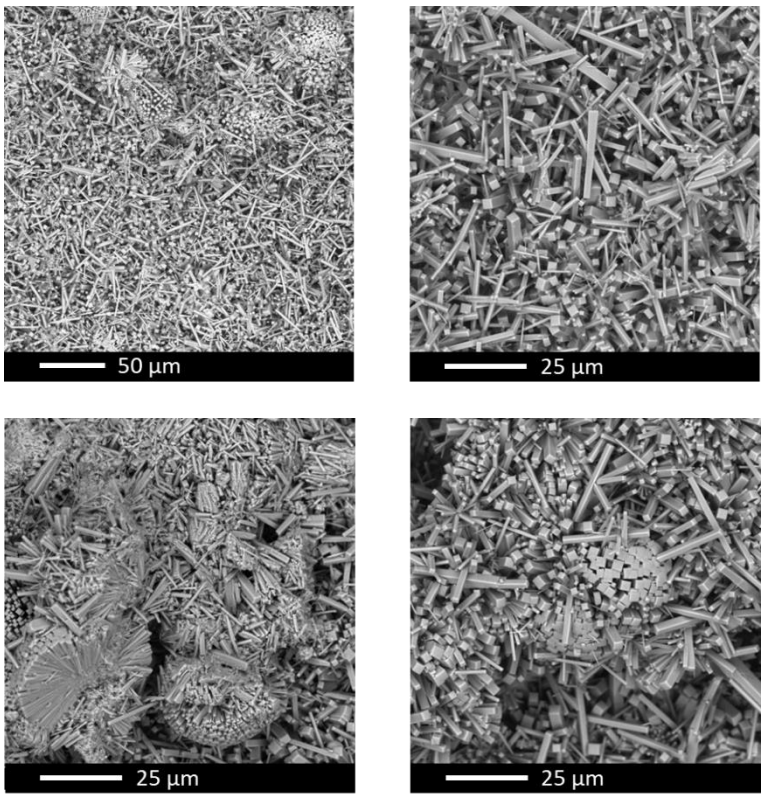

Figure 9. SEM micrographs of the surface of the beryllium samples corroded in MPC solution for one year.

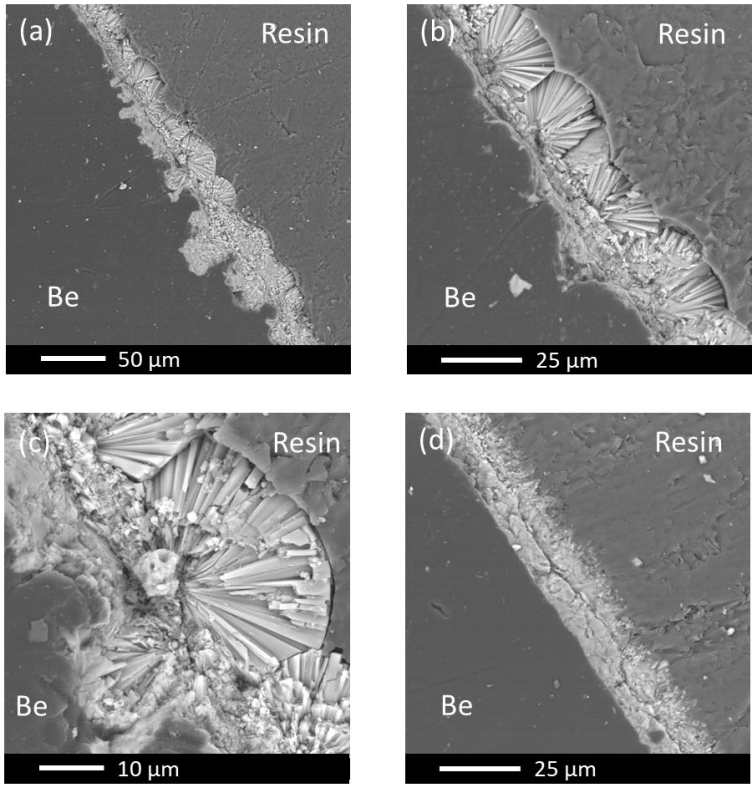

Figure 10. SEM micrographs of the cross section of the beryllium corroded in MPC solution for one year.

Table 8. Point EDS analysis of the corrosion product and crystals present at the surface of the beryllium after one year of corrosion in MPC solution.

Average atomic %	**O**	**K**	**P**	**Si**	**Mg**	**Ca**
Corrosion product layer	45.3	17.6	27.3	0.7	1.1	6.7
Crystals	67.9	12.5	18.6	0.0	0.0	0.4
Average weight %	**O**	**K**	**P**	**Si**	**Mg**	**Ca**
Corrosion product layer	30.4	25.3	31.4	0.8	1.1	9.9
Crystals	50.8	21.9	26.0	0.0	0.0	0.7

Figure 11 shows SEM micrographs of the precipitates found at the bottom of the test containers. They were composed of needle-like particles similar to the crystals present at the surface of the beryllium samples and it is assumed that the composition is also similar. Unfortunately, not enough crystals could be recovered to make XRD analysis on the crystals.

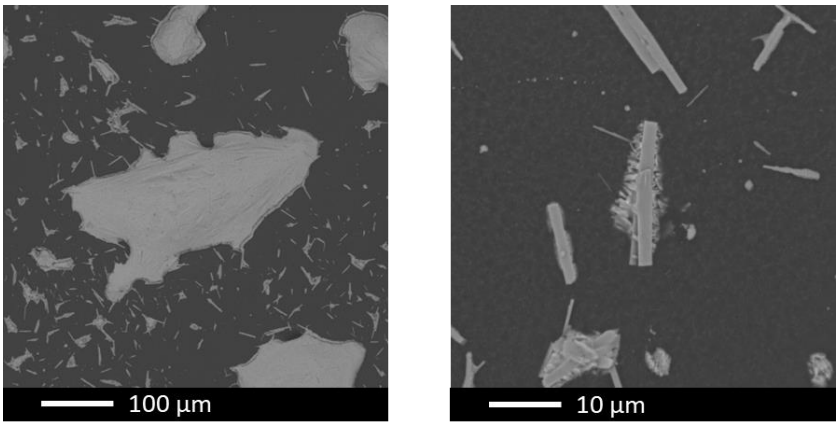

Figure 11. SEM micrographs of precipitates observed at the bottom of the container after the beryllium corrosion test in MPC solution.

Finally, XRD patterns were recorded after corrosion of beryllium in OPC and MPC solutions for one year (Figure 12). As expected, because no (or only a very thin) corrosion product layer was formed at the surface of the beryllium after corrosion in OPC solution, only beryllium and beryllium oxide were measured by XRD. In the MPC solution, however, in addition to Be and BeO, $KBePO_4 \cdot H_2O$ was also detected. This phase has an orthorhombic crystal structure, corresponding to the needle-like shape of the crystals formed.

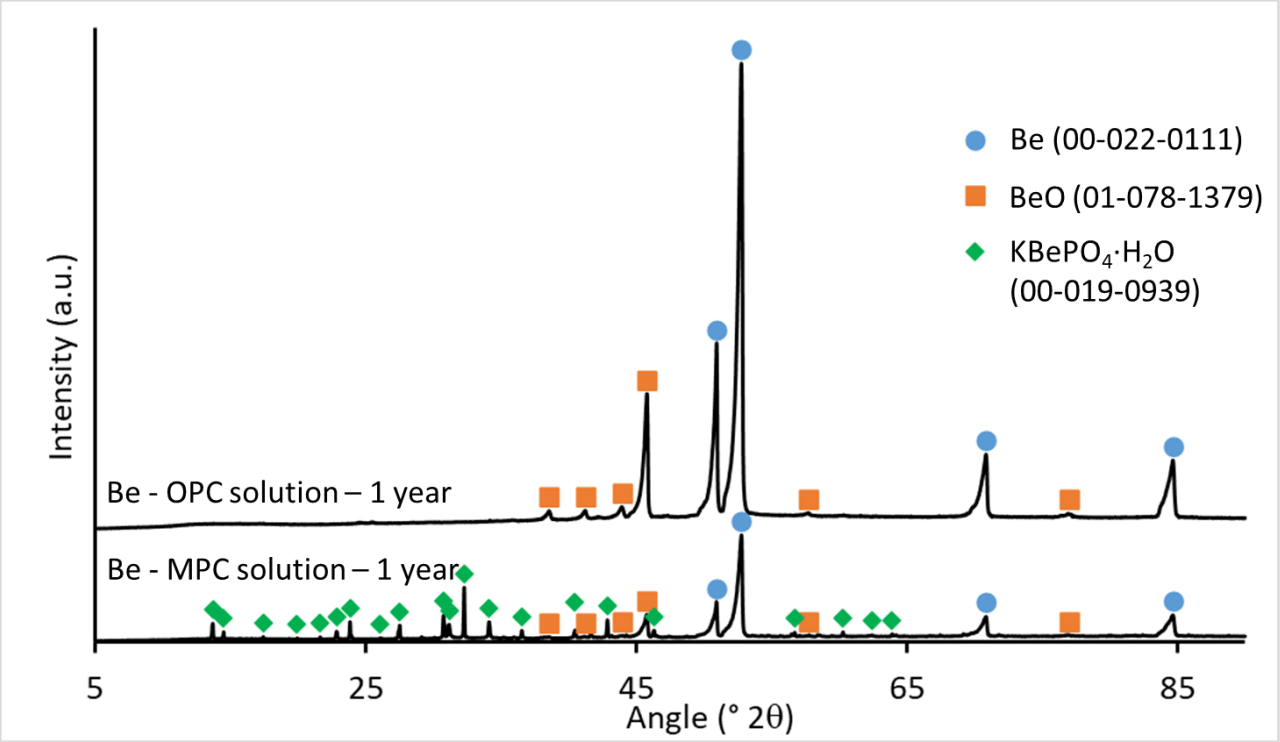

Figure 12. XRD patterns of beryllium metal corroded for one year in OPC and MPC solutions.

3.1.3 Weight loss and ICP-MS measurements

Within the framework of this project, in FZJ, the beryllium corrosion rate was measured using two direct methods, namely, measurements of mass loss of the initial samples (ML) and the concentration of beryllium in solution (ICP-MS). However, the mass loss of the samples during corrosion at near neutral conditions and at pH less than 13 is insignificant and is maintained at the level of experimental measurement accuracy (Figure 13a). For example, at pH = 12.54, the change in the mass of the sample during the first three weeks remains constant and equal to zero. A slight decrease in the mass of the sample takes place only during the fourth week. For the sample under study at pH = 6.71, a slight but stable increase in mass is observed. At the same time, the content of beryllium in solution for all experiments is well measurable and increases with the duration of the experiment (Figure 13b).

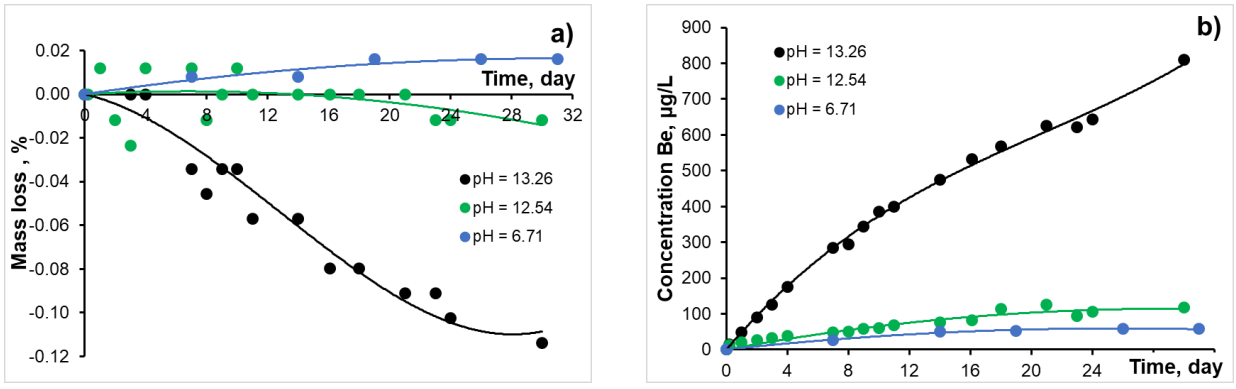

Figure 13. a) Sample mass loss (ML) and b) concentration of beryllium in solution in experiments at pH 6.71, 12.54, 13.26 as function of exposure time.

Ideally, the values of the corrosion rates determined by these two methods (ML and ICP-MS) should be equal. However, it has been shown that for all experiments, the corrosion rate values determined from the measurement of the beryllium content in solutions (ICP-MS) are always lower than those determined by the change in the mass (ML) of the initial samples.
This difference can be explained by the formation of a hydroxide layer on the surface of the samples during the corrosion process, limiting the beryllium concentration in solution. This is particularly evidenced by the increase in the mass of the sample during corrosion experiments at pH = 6.71 (Figure 13a). The formation of a hydroxide layer at the corrosion points in these experiments is confirmed by optical microscope studies (Figure 14(a and b)). In addition, the formation of a hydroxide layer at pH = 13.99 is confirmed by SEM (Figure 14c).

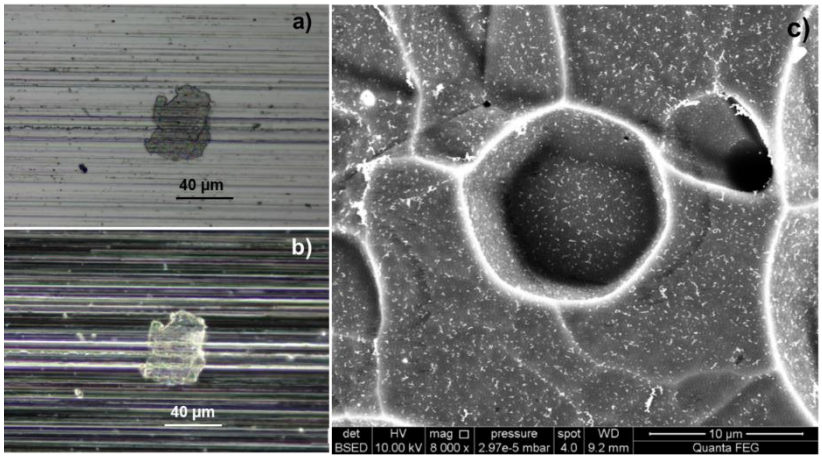

Figure 14. Optical images of the beryllium sample surface corroded at pH 6.71 in a) normal and b) polarized light, c) SEM micrograph (back scattered electron mode) of the beryllium sample surface corroded at pH 13.99.

The presence of a hydroxide layer on the metal surface leads to an underestimation of the amount of corroded metal by measuring ML:

$$\mathrm{ML} = -\mathrm{m}_{\mathrm{Be}}^{\mathrm{cor}} + \mathrm{Rm}_{\mathrm{Be}}^{\mathrm{s}} \qquad \text{(Equation 7)}$$

where $\mathrm{m}_{\mathrm{Be}}^{\mathrm{cor}}$ is the mass of corroded beryllium and $\mathrm{m}_{\mathrm{Be}}^{\mathrm{s}}$ is the mass of beryllium being in the form of hydroxide on the sample surface, and the coefficient R = 4.774 equals the ratio of the molecular weight of the hydroxide and the metal, respectively.

The mass of corroded beryllium consists of two components – the mass of beryllium as hydroxide on the metal surface and that dissolved in solution ($\mathrm{m}_{\mathrm{Be}}^{\mathrm{sol}}$).

$$\mathrm{m}_{\mathrm{Be}}^{\mathrm{cor}} = \mathrm{m}_{\mathrm{Be}}^{\mathrm{s}} + \mathrm{m}_{\mathrm{Be}}^{\mathrm{sol}} \qquad \text{(Equation 8)}$$

Using Equation 7 and Equation 8, Equation 9 can be obtained for the mass of corroded beryllium, which consists of two experimentally measured values – the concentration of beryllium in solution (determined by ICP-MS) and the mass loss (ML).

$$\mathrm{m}_{\mathrm{Be}}^{\mathrm{cor}} = \frac{\mathrm{Rm}_{\mathrm{Be}}^{\mathrm{sol}} + \mathrm{ML}}{\mathrm{R}-1} \qquad \text{(Equation 9)}$$

An example of processing experimental data on mass loss (ML) and beryllium content (ICP-MS) in solution in order to determine the corrosion rate is shown in Figure 15 for the representative case of a corrosion experiment performed at pH = 13.42.

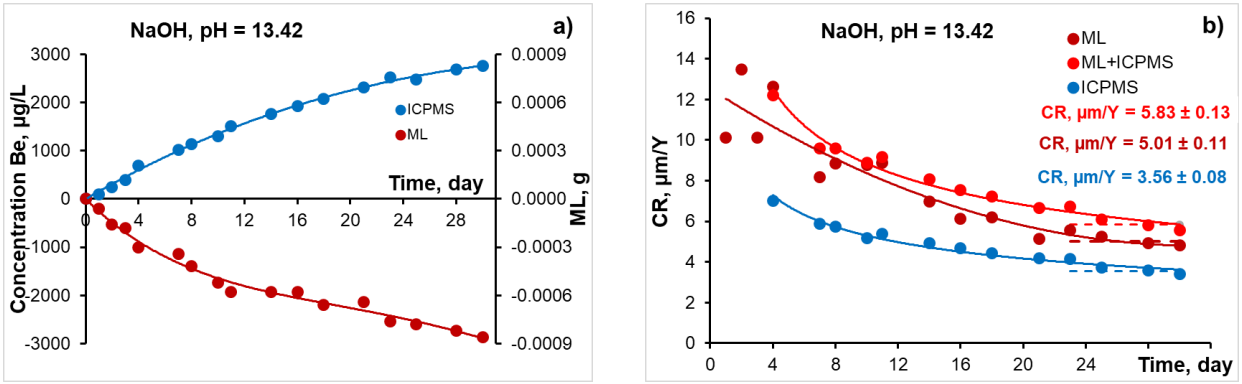

Figure 15. a) Sample mass loss (ML) and concentration beryllium in solution in representative experiment at pH 13.42, as function of exposure time, b) corrosion rate measured by 3 methods (ML, ICPMS, ML+ICPMS) as function of exposure time.

In Figure 15a, the measured mass loss (ML) and concentration of beryllium in solution (ICP-MS) are shown for a representative experiment performed at pH = 13.42 as function of experimental duration. The mass of the sample decreases (brown line) and the beryllium content in solution (blue line) increases monotonically with increasing duration of the experiment. Based on these data, the corrosion rates (CR) were calculated; the results are presented in Figure 15b (brown and blue lines, respectively). The value of corrosion rates and their experimental error were calculated specifically for the last three experimental points and is equal to 5.01 ± 0.11 µm/y and 3.56 ± 0.08 µm/y, respectively.

The evolution of the beryllium corrosion rate, taking into account the presence of a hydroxide layer (Equation 9), is shown in Figure 15b (red line). The value of the average corrosion rate after 30 days is 5.83 ± 0.13 µm/y. The corrosion rate determined by our method is higher than the ones determined by the measurements (ML and ICP-MS). Because in the case of mass loss measurements, the increase in the mass of the sample due to the presence of a hydroxide layer on the surface of the sample is not taken into account. The beryllium content in the solution also does not take into account the beryllium contained in this layer.

It should be particularly noted that the proposed combined method makes it possible to determine the corrosion rates of beryllium at neutral pH values when the change in the mass of the sample is close to zero or even positive. That is, even in cases where measuring the corrosion rate solely by the ML method is impossible.

The results of the corrosion rate measurements at various pH values are presented in Figure 16 and summarized in Table 9. Under alkaline conditions, the corrosion rates of beryllium in logarithmic coordinates increase linearly with increasing pH and correlate well with the results obtained for beryllium corrosion in the Ordinary Portland Cement pore water measured using this technique and when measuring the release of H_2 (see Section 3.1.3).

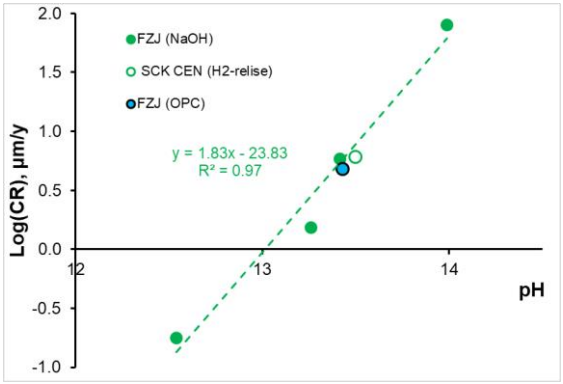

Figure 16. Corrosion rates of metallic beryllium.

Table 9. Corrosion rates (CR) of metallic beryllium in NaOH solutions of different pH.

media	Duration, days	pH	CR, µm/Y
NaOH	30	6.71	0.16 +/- 0.01
NaOH	30	12.54	0.18 +/- 0.01
NaOH	30	13.26	1.54 +/- 0.01
NaOH	30	13.42	5.8 +/- 0.1
NaOH	30	13.99	79 +/- 1

In Figure 17a, the measured mass loss and concentration of beryllium in solution are shown as function of experimental duration for an experiment performed in Ordinary Portland Cement pore water (pH = 13.43). The mass of the sample decreases (brown line) and the beryllium content in solution (blue line) increases monotonically with increasing duration of the experiment. Based on these data, the corrosion rates (CR) were calculated by the combined method (ICP-MS and ML); the results are presented in Figure 17b (black line). The corrosion rates are 4.8 ± 0.2 µm/y and 1.90 ± 0.09 µm/y, for an experimental duration of 30 and 120 days, respectively.
For comparison, Figure 17b also shows the dependence of the beryllium corrosion rate for a NaOH solution with a pH of 13.42 (red line). At similar pH values, the corrosion rate of beryllium in an OPC pore water is slightly lower than in NaOH based solution for an experimental duration of 120 days (CR = 2.84 ± 0.13 µm/y).

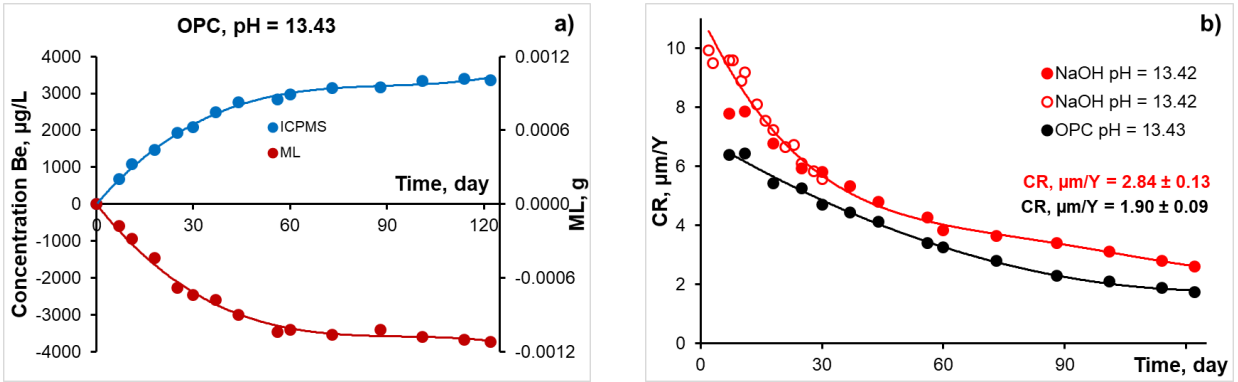

Figure 17. a) Sample mass loss (ML) and concentration of beryllium in OPC pore water at pH 13.43, as a function of exposure time, b) corrosion rates of beryllium in OPC pore water and NaOH solution (pH=13.42) with similar pH as a function of exposure time.

The appearance of the samples after corrosion tests in the magnesium phosphate cement pore water (MPC solution, pH = 7.91) and the magnesium phosphate cement pore water with the addition

of boric acid (MPC+B solution, pH = 7.73) are shown in Figure 18a and Figure 18c, respectively. It can be seen that during the corrosion process, an additional layer of black or grey material is formed on the surface of the samples. For the beryllium sample after corrosion in MPC solution, the thickness of this layer is very significant.

In Figure 18b and Figure 18d, the measured mass loss and concentrations of beryllium in solution are shown as function of experimental duration for experiments performed in MPC and MPC+B pore water, respectively. In both cases, the beryllium content in solution increases monotonically, but the beryllium content in the MPC solution is about two times higher than in the MPC+B solution.

The mass of the sample (brown line) first decreases, and then increases monotonically with increasing duration of the experiment, Figure 18b and Figure 18d. The most significant increase occurs for the sample that was tested in MPC pore water, Figure 18b. The minimum in the mass loss of the sample is observed after 30 days and is equal to - 0.0004g, then the mass of the sample increases by 0.004g. This increase is due precisely to the growth of the near-surface cover layer.

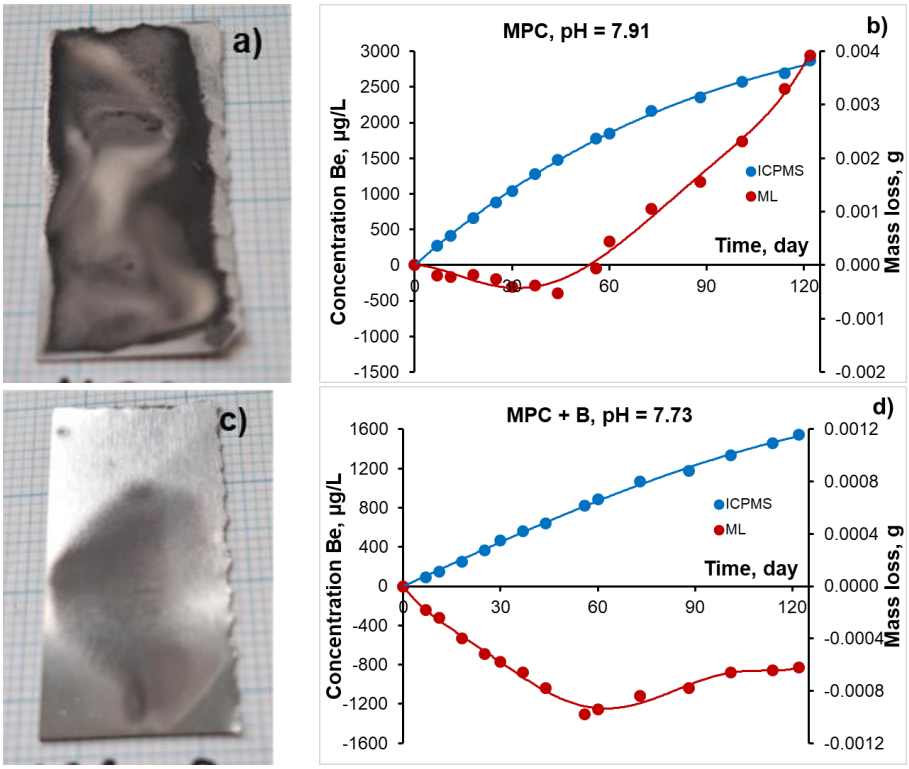

Figure 18. a) and c) Images of beryllium samples after corrosion experiments in MPC and MPC+B pore water, respectively, b) and d) mass loss (ML) and concentration of beryllium in MPC and MPC+B pore water as a function of exposure time, respectively.

Thus, we can assume that the measured value of mass loss (ML) consists of two components, namely, a decrease in mass occurs due to corrosion of beryllium (ML*), and an increase in mass occurs due to the growth of the cover layer (M_{covL}), as mentioned in Equation 10.

$$ML = ML^{*} + M_{covL} \qquad \text{(Equation 10)}$$

The dependence of the mass of the cover layer (M_{covL}) on the duration of the experiment can be estimated as follows. The experimental data for ML (the increasing part after 30 days) is well described by the cubic equation (red line in Figure 19a). Then the dependence of the mass of the cover layer (M_{covL}) on the duration of the experiment is a given quadratic equation without a free term (red line in Figure 19b). The dependence of the mass of the corroded beryllium (ML*) on the

experimental duration is determined from Equation 10 and is shown in Figure 19b as a brown dotted line.

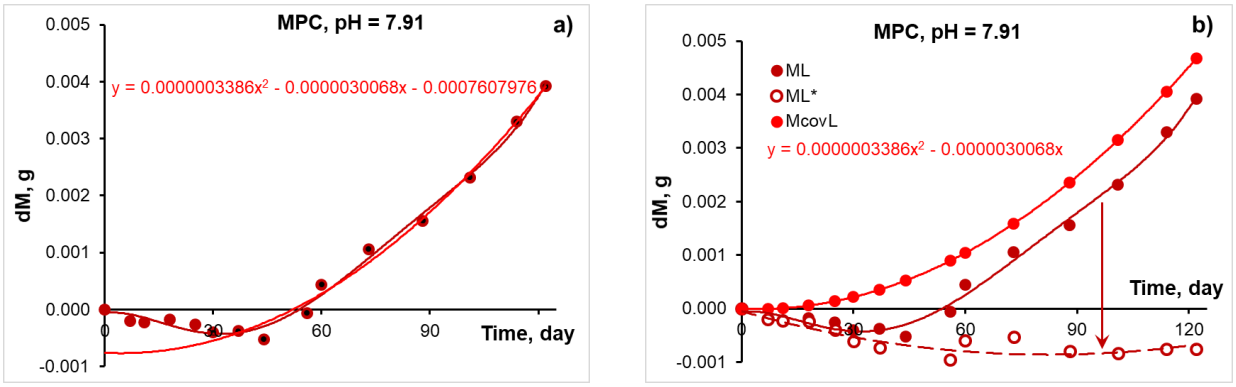

Figure 19. a) Beryllium sample mass change (dM) as a function of experiment time (brown line), approximation with quadratic equation (red line) b) separating functions of beryllium mass loss (ML, empty brown points, dashed line) and covered layer mass increase (red line) as a function of time.*

Thus, the mass of corroded beryllium (ML^*, m_{Be}^{cor}) consists of two components, namely beryllium in solution (m_{Be}^{sol}) and beryllium included in the cover layer (m_{Be}^{covL}) (Equation 11).

$$ML^* = m_{Be}^{cor} = m_{Be}^{sol} + m_{Be}^{covL} \qquad \text{(Equation 11)}$$

As mentioned in Section 3.1.2.2, the cover layer is composed of $BeKPO_4 \cdot H_2O$. Therefore, the content of beryllium in the cover layer can be determined from the ratio of the molecular weights of beryllium (9.0122 g/mol) and this compound (161.1009 g/mol) (Equation 12).

$$m_{Be}^{covL} = 0.05594 M_{covL} \qquad \text{(Equation 12)}$$

In Figure 20a, the calculated mass loss (ML*) of the corroded beryllium and the concentration of beryllium in solution are shown as function of experimental duration for an experiment performed in MPC pore water (pH = 7.91). The mass of the corroded beryllium decreases (brown line) and the beryllium content in solution (blue line) increases monotonically with increasing duration of the experiment.

In Figure 20b, the calculated mass of beryllium in the cover layer (m_{Be}^{covL}, yellow line), the mass of beryllium in solution (m_{Be}^{sol}, blue line) and the mass of corroded beryllium (m_{Be}^{cor}, red line) are shown as function of experimental duration for the experiment performed in MPC pore water. All these dependencies are increasing monotonically with increasing duration of the experiment. It should be noted that despite the fact that the cover layer is quite thick (massive), the beryllium content in this layer is insignificant and significantly lower than the mass of dissolved beryllium (approximately 2.5 times).

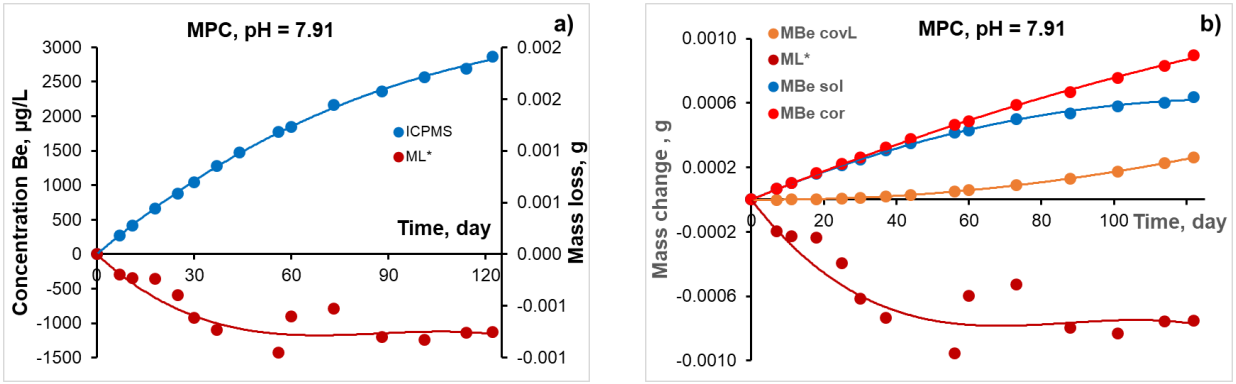

Figure 20. a) Sample mass loss (ML) and concentration of beryllium in MPC pore water at pH 7.91, as a function of exposure time, b) sample mass loss (ML*, brown line) and mass of beryllium in solution (blue line), in cover layer (yellow line) and total mass of corroded beryllium (red line) as function of exposure time.*

According to Equation 11, the mass of corroded beryllium (m_{Be}^{cor}) should be equal to the recalculated mass loss (ML*). The dependences of these parameters on the duration of corrosion are shown in Figure 21a. In addition, Figure 21a presents the difference between these parameters (green points) and shows that it does not exceed the values of the experimental measurement error (black horizontal dotted lines) for most of the experimental data. This indicates the correctness of our assumptions regarding the amount and composition of the cover layer and the features of beryllium corrosion in these types of solutions (MPC).

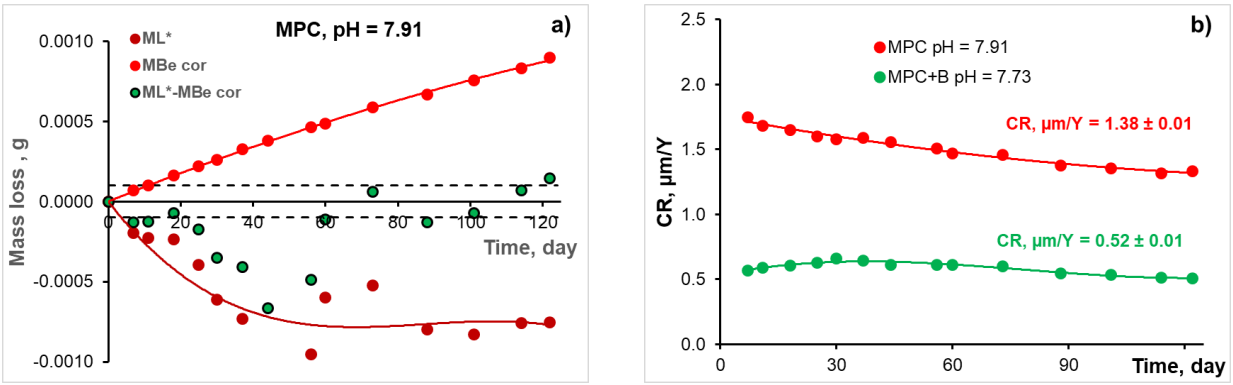

Figure 21. a) Sample mass loss (ML, brown line) and total mass of corroded beryllium (red line) and their difference (green dots) as a function of exposure time, b) corrosion rate of beryllium in MPC and MPC+B pore water as a function of exposure time.*

Based on these data, the corrosion rates (CR) were calculated and the results are presented in Figure 21b. The corrosion rates are 1.38 ± 0.01 µm/y and 0.52 ± 0.01 µm/y for the MPC and MPC+B pore water, respectively. It can be seen that even small additions of boric acid to MPC pore water significantly (2.7 times) reduces the corrosion rate of beryllium.

The results of measurements of the beryllium corrosion rates for OPC, MPC, MPC+B pore water solutions and for NaOH based solutions with similar pH are summarized in Table 10.

.

Table 10. Corrosion rates (CR) of metallic beryllium in OPC, MPC, MPC+B and NaOH solutions.

media	pH	CR, µm/Y		
		30 days	122 days	ratio
NaOH	13.42	5.8 +/- 0.1	2.84 +/- 0.13	2.0
OPC	13.43	4.8 +/- 0.2	1.90 +/- 0.09	2.5
MPC	7.91	1.60 +/- 0.01	1.38 +/- 0.01	1.2
MPC + B	7.73	0.64 +/- 0.01	0.52 +/- 0.01	1.2
NaOH	6.71	0.16 +/- 0.01	0.040 +/- 0.002	4.0

The results of all our corrosion rate measurements (duration 30 days) are presented in Figure 22. Under alkaline conditions (pH > 12), the corrosion rates of beryllium in logarithmic coordinates increase linearly with increasing pH.

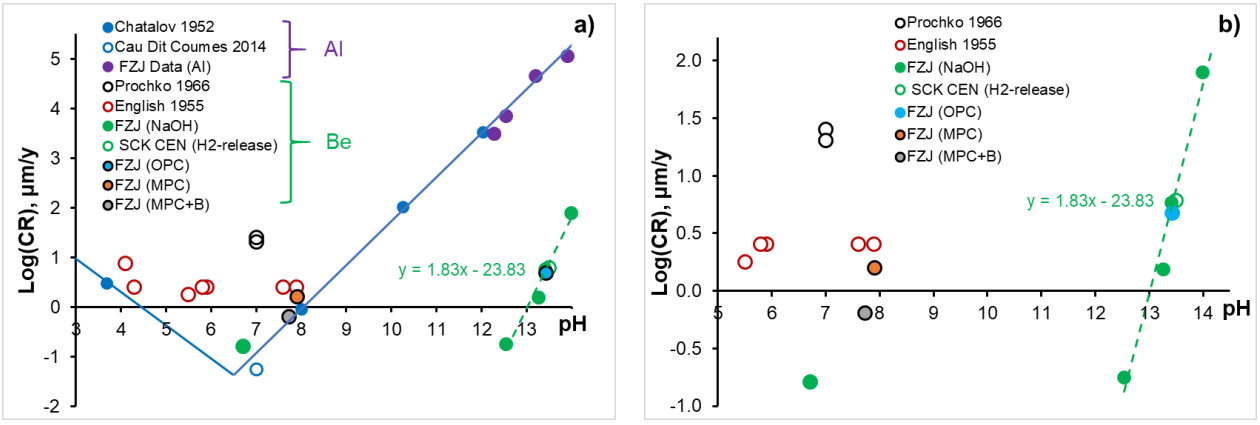

Figure 22. Corrosion rates of metallic beryllium and aluminium determined in this study compared to available literature data [19-22].

For comparison, the measured corrosion rates of metallic Al determined under similar conditions are also included in Figure 22 and Table 11 [23]. The measured corrosion rates show also a strong increase with increasing pH, in good agreement with literature data [22], and are significantly higher than the corrosion rates of metallic beryllium. The ratios of corrosion rates for metallic aluminium and beryllium (CR_{Al} / CR_{Be}) reveal that the corrosion rates of metallic aluminium are 3 to 4 orders of magnitude higher than those of beryllium (Table 11). This indicates that metallic aluminium is not a suitable analogue to assess the behaviour of beryllium under highly alkaline cementitious conditions.

Table 11. Corrosion rates (CR) of metallic beryllium and aluminium in NaOH solutions of different pH.

pH	CR, µm/y		CR_{Al}/CR_{Be}
	Al	Be	
12.54	6940 +/- 20	0.18 +/- 0.01	38556
13.26	45730 +/- 50	1.54 +/- 0.01	29695
13.99	112800 +/-100	79 +/- 1	1428

The decrease in beryllium corrosion rates with time in NaOH based solutions and OPC pore water is presumably due to a hydroxide layer forming on the surface of the beryllium metal, which is confirmed by our microscopic studies (Figure 14). The good adhesion of beryllium hydroxide to the metal surface is probably due to similarities of their crystal lattice parameters (a_{Be} = 2.287Å [24] ≈ $0.25(a + b)_{Be(OH)2}$ = 2.288Å [25]). Moreover, the hydroxide occupies a volume 4.54 times larger than that of the metal consumed in forming the hydroxide (Pilling–Bedworth ratio). Thus, being in expansion, the oxide does not have any tendency to spall. The presence of a protective layer of

hydroxide on the surface of the material probably determines the higher corrosion resistance of metallic beryllium in comparison to aluminium under hyperalkaline conditions.
The literature data on beryllium corrosion in neutral and slightly acidic solutions [20, 21] are included in Figure 22 for comparison. It should be noted that these data are for neutral and slightly acidic solutions and estimates of the corrosion rates rather than accurately measured values. Data from [20] shows that corrosion rate remains constant in a wide pH region (from pH = 4 to pH = 8) and equals 2.54 µm/y. Our value of corrosion rate at pH = 6.71 (duration of 4 months) is lower and equals 0.040 µm/y. This difference could be explained by the different temperature used in the corrosion experiments. In our study corrosion experiments were conducted at room temperature, while in [20] at 80°C.
Despite the large difference in solution pH, the difference between corrosion rates in OPC and MPC solutions is rather small: 1.90 µm/y for OPC, and 1.39 µm/y for MPC. Small additions of boric acid to MPC pore water distinctly decrease the corrosion rate down to 0.52 µm/y. Note that while corrosion rates in OPC solution are similar for pure beryllium foils and S-200-F grade beryllium pellets, results differ in MPC solution. The S-200-F grade beryllium pellets corroded at the much higher rate (close to 10-15 µm/y (see Sections 3.1.1.2 and 3.1.2.1)). More tests will be needed to explain these differences.

3.1.3.1 SEM observations of samples corroded in high pH NaOH solutions

According to West [26], corrosion of beryllium metal starts at sensitive points, which comprise crystallographic defects, cavities, or scratches in the metal surface and/or impurity inclusions mainly localized along grain boundaries [27]. Figure 23a shows the surface of the original beryllium foil with two types of mechanical defects visible on the surface of the beryllium metal, namely numerous elongated linear defects (scratches) due to mechanical processing (rolling) and, locally present, rather deep defects (cavities). Impurity inclusions are also present in the material with sizes varying between 0.4 to 3.5 µm (cf. Figure 23a). These inclusions were identified by SEM-EDS as BeO, Be_2C, silicon (Si), and various intermetallic phases such as Be/Cr/Al/Mn, Si_2Cr and Al/Mn/Si/Cr.

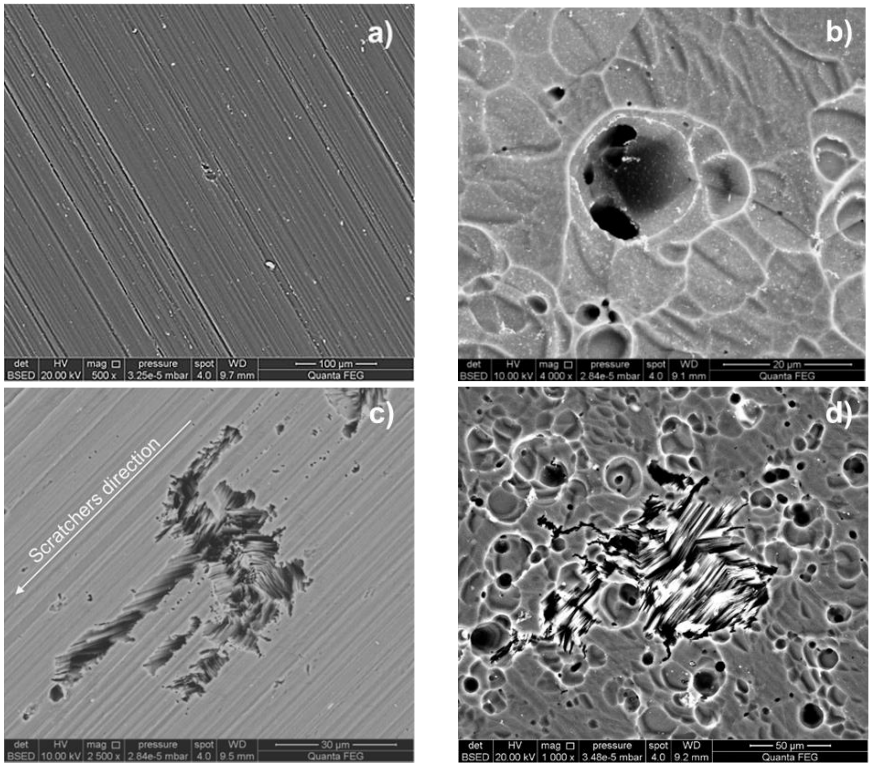

Figure 23. a) SEM surface images (back-scattered electron images) of a pristine beryllium sample with scratches from mechanical processing and impurity inclusions (white spots); b) beryllium hydroxide layer formed on a beryllium sample corroded at pH 13.99; c) corrosion pits in beryllium metal corroded at pH 13.22, and d) pH 13.99.

Figure 23b shows that the surface of the corroded beryllium metal samples is uniformly covered by a thin layer of $Be(OH)_2$. Moreover, two types of corrosion pits could be observed in the corroded samples: (i) large (40 – 200 µm) pits with an elongated shape, where the direction of pit elongation coincides with the direction of the original scratches (Figure 23c), and (ii) smaller (3 – 30 µm) corrosion pits characterized by a spherical (cylindrical) shape (cf. Figure 23d).
Apparently, the large corrosion pits formed at the sites of originally present scratches and cavities. They have a complex morphology consisting of pit walls and parallel plates, which can be explained by the differing dissolution rates of different crystallographic orientations of the beryllium grains [28]. The small corrosion pits are also located on the tops of scratches and irregularities of the original beryllium metal. This indicates that mechanical defects (cavities, edges of scratches) in the initial beryllium foil are the initiation places for pitting corrosion.

3.2 Corrosion tests in cement pastes and mortars

3.2.1 Electrochemical measurement (EIS)

3.2.1.1 Evolution of the Nyquist and Bode diagrams[8]

As explained in Section 2.2.3, two different tests were performed per cement paste/mortar type. In the first test, the electrodes were immersed in a vial filled with cement paste/mortar. In the second test, hardened[9] cement pastes containing the electrodes were immersed in OPC or MPC pore water solution.

[8] Note that this information represents only one of the triplicate tests. However, the corrosion rate (see Section 3.2.1.2) was calculated using the average value of R_t of the three tests.
[9] Hardened in glove box under argon atmosphere for 1 day before immersion in solution.

3.2.1.1.1 Beryllium corrosion in OPC paste and OPC paste immersed in OPC solution

The evolution of the Nyquist and Bode diagrams of beryllium metal exposed to OPC paste and to OPC paste immersed in OPC solution in function of time are shown in Figure 24 and Figure 25, respectively. The fitting values, using the EEC described in Figure 1c, are given in Table 12 and Table 13, respectively. The shape of the Nyquist plots of both tests was similar. However, at high frequencies (Figure 24b, Figure 25b, Table 12 and Table 13), corresponding to the response of the cement matrix, a larger impedance, as well as a larger resistance of the non-conductive pore path (R_{ncp}), were observed when OPC pastes were not immersed in solution. This could result from the lower water availability in the cement paste pores, compared to the test in OPC immersed in OPC solution. Note that the resistance of the conductive pore path (R_{cp}) of the system OPC immersed in OPC solution dramatically increased after 105 days (Table 13). This could reveal pore clogging due to the precipitation of salt from the solution or corrosion products in the pores of the cement paste. More tests are however needed to prove this statement. The evolution of R_t also differs in both tests. In the OPC paste system, R_t increased during the entire period of testing (from ~4.1×10^5 to 2.9×10^6 Ω). However, in the system OPC paste immersed in OPC solution, R_t increased during the first 14 days after which it stabilised at values around 1.4×10^6 Ω until the end of the test (135 days). The Bode plots also revealed an increase of the impedance modulus with time at low frequencies (Figure 24c and Figure 25c), while the phase angle peak slightly shifted with time to lower frequencies, for both systems (Figure 24d and Figure 25d).

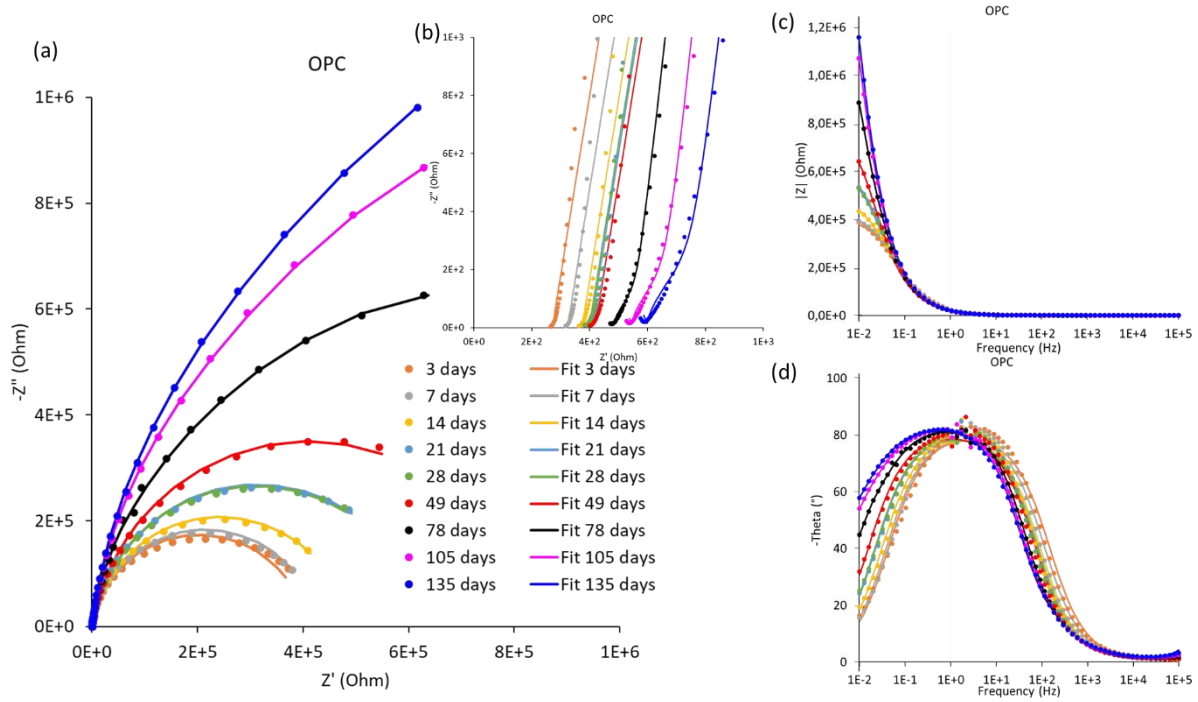

Figure 24. (a and b) Evolution of the Nyquist spectra and (c and d) evolution of the Bode spectra of beryllium in OPC paste in function of time (dots: experimental results; lines: fit).

Table 12. Fitting data of the EIS spectra of beryllium in OPC paste.

Days	CPE_m		R_{cp} (Ω)	R_{ncp} (Ω)	CPE_{ncp}		CPE_{dl}		R_t (Ω)
	K_m ($F \cdot S^{\alpha}$)	α_m			K_{ncp} ($F \cdot S^{\alpha}$)	α_{ncp}	K_{dl} ($F \cdot S^{\alpha}$)	α_{dl}	
3	5.1×10^{-14}	0.9	270	7570	2.6×10^{-9}	0.9	8.0×10^{-6}	0.9	406210
7	9.8×10^{-11}	0.9	325	9855	2.0×10^{-9}	0.9	8.3×10^{-6}	0.9	428790
14	1.4×10^{-10}	0.9	375	10265	3.1×10^{-9}	0.9	8.9×10^{-6}	0.9	485540
21	2.3×10^{-10}	0.9	405	9740	4.8×10^{-9}	0.9	9.1×10^{-6}	0.9	628380
28	2.8×10^{-10}	0.9	400	9140	6.0×10^{-9}	0.9	9.5×10^{-6}	0.9	622270
49	2.5×10^{-10}	0.9	420	9135	7.7×10^{-9}	0.9	9.8×10^{-6}	0.9	820310
78	4.3×10^{-10}	0.9	515	6385	3.1×10^{-8}	0.9	9.6×10^{-6}	0.9	1448200
105	5.5×10^{-10}	0.9	595	5700	4.9×10^{-8}	0.9	9.2×10^{-6}	0.9	2315900
140	6.6×10^{-10}	0.9	675	4740	8.5×10^{-8}	0.9	8.9×10^{-6}	0.9	2914700

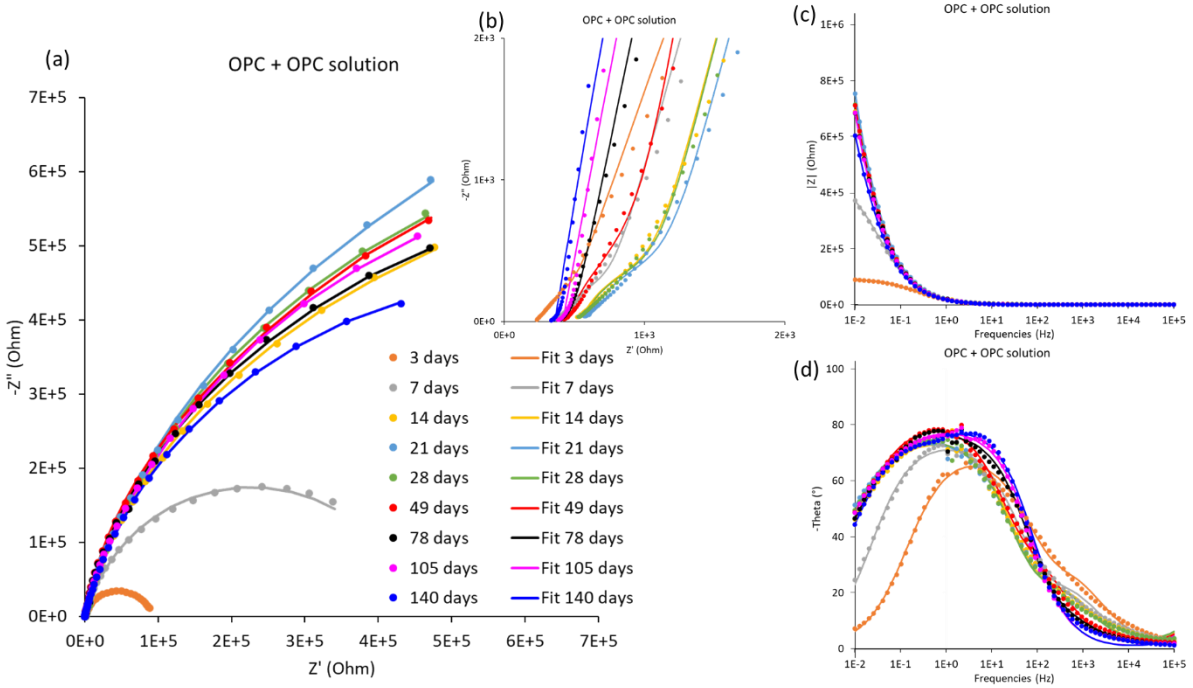

Figure 25. (a and b) Evolution of the Nyquist spectra and (c and d) evolution of the Bode spectra of beryllium in OPC paste immersed in OPC solution in function of time (dots: experimental results; lines: fit).

Table 13. Fitting data of the EIS spectra of beryllium in OPC paste immersed in OPC solution.

Days	CPE_m		R_{cp} (Ω)	R_{ncp} (Ω)	CPE_{ncp}		CPE_{dl}		R_t (Ω)
	K_m ($F \cdot S^{\alpha}$)	α_m			K_{ncp} ($F \cdot S^{\alpha}$)	α_{ncp}	K_{dl} ($F \cdot S^{\alpha}$)	α_{dl}	
3	1.7×10^{-9}	0.9	470	500	1.5×10^{-6}	0.8	1.2×10^{-5}	0.81	92980
7	1.3×10^{-9}	0.9	735	865	1.1×10^{-6}	0.8	1.1×10^{-5}	0.84	451750
14	1.1×10^{-9}	0.9	950	1340	3.4×10^{-7}	0.9	1.0×10^{-5}	0.83	1294600
21	1.1×10^{-9}	0.9	1040	1480	3.3×10^{-7}	0.9	1.0×10^{-5}	0.83	1710300
28	1.2×10^{-9}	0.9	980	1345	3.7×10^{-7}	0.9	1.1×10^{-5}	0.84	1501200
49	1.1×10^{-9}	0.9	775	1120	1.1×10^{-6}	0.9	1.0×10^{-5}	0.88	1256500
78	6.6×10^{-10}	0.9	480	2575	1.1×10^{-7}	0.9	1.1×10^{-5}	0.86	1206900
105	1.2×10^{-9}	0.9	66315	420	4.3×10^{-5}	0.9	1.4×10^{-5}	0.88	1370800
140	1.2×10^{-9}	0.9	22835	365	4.6×10^{-5}	0.9	1.4×10^{-5}	0.89	995500

The evolution of the Nyquist and Bode diagrams of beryllium metal exposed to MPC mortar and to MPC mortar immersed in MPC solution in function of time are shown in Figure 26 and Figure 27, respectively. The fitting values, using the EEC described in Figure 1d, are given in Table 14 and Table 15, respectively.

The shape of the Nyquist plots corresponding to samples corroding in MPC mortar changed with time (Figure 26 (a and b)). The semi-circle present at high frequency, corresponding to the mortar matrix, appeared after 14 days and then its diameter increased with time. This is also observed in the Bode plot of the impedance in function of the frequency (plateau at high to medium frequencies in Figure 26c). Moreover, the peaks in the Bode plots of the phase angle in function of the frequency shifted to lower frequency (Figure 26d).

At lower frequencies, the impedance showed a capacitive effect (Figure 26a), corresponding to the passivation of the beryllium electrode, as shown also by the high value of R_t (10^6-10^7 Ω) during the whole period of the test (Table 14). Note that capturing valid EIS data became more and more difficult with time as noise appeared in the EIS spectra, making it sometimes impossible to obtain any valuable signal. This was attributed to the lower amount of water present in the system.

Looking at the tests performed in MPC mortar immersed in MPC solution (Figure 27), the EIS spectra showed a different shape than the ones performed in MPC mortar. The important amount of water present in the system seems to decrease the impedance of the MPC mortar (no or little semi-circle at high frequencies of the Nyquist plots (Figure 27 (a and b)) and no plateau at high to medium frequencies in Figure 27c), while the capacitive effect corresponding to the passivation of the beryllium electrode is still clearly visible (Figure 27 (a and b)). Note that the R_t value remains similar as the one observed for beryllium embedded in MPC mortar.

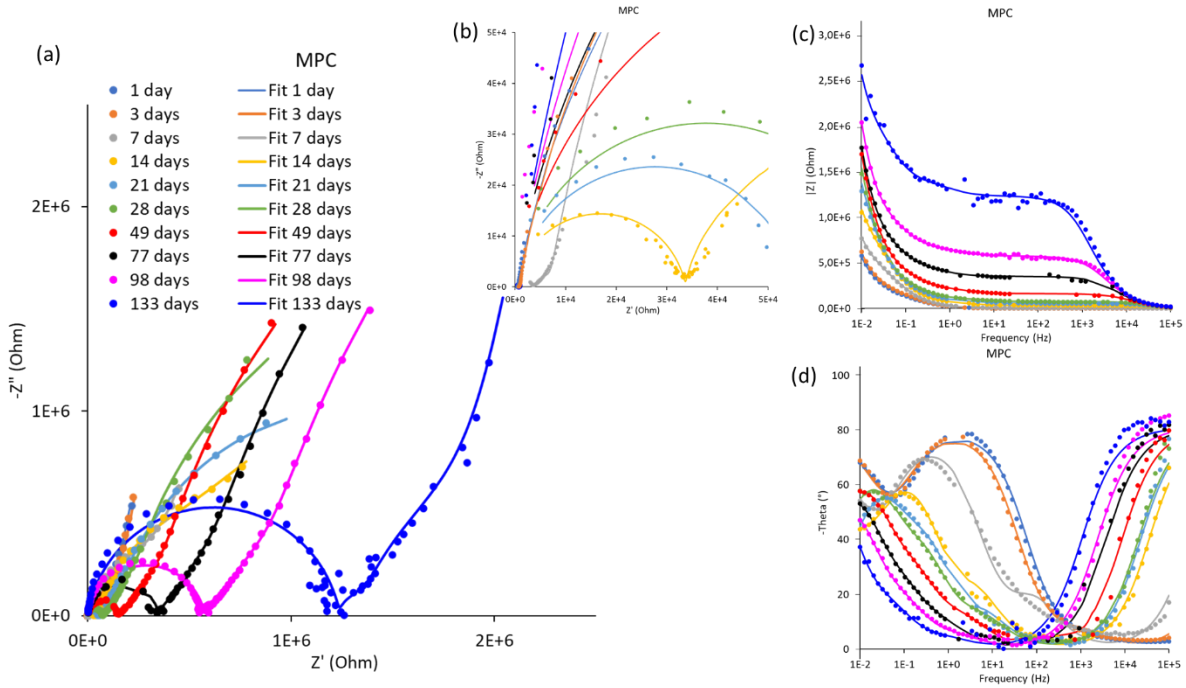

Figure 26. (a and b) Evolution of the Nyquist spectra and (c and d) evolution of the Bode spectra of beryllium in MPC mortar in function of time (dots: experimental results; lines: fit).

Table 14. Fitting data of the EIS spectra of beryllium in MPC mortar.

Days	CPE_m		R_{cp} (Ω)	R_{ncp1} (Ω)	CPE_{ncp1}		R_{ncp2} (Ω)	CPE_{ncp2}		CPE_{dl}		R_t (Ω)
	K_m ($F \cdot S^{\alpha}$)	α_m			K_{ncp1} ($F \cdot S^{\alpha}$)	$\alpha_{nc\ p1}$		K_{ncp2} ($F \cdot S^{\alpha}$)	$\alpha_{nc\ p2}$	K_{dl} ($F \cdot S^{\alpha}$)	α_{dl}	
1	7.3×10^{-10}	0.9	1.3×10^{5}	560	1.4×10^{-5}	0.9	3820	3.3×10^{-8}	0.9	2.3×10^{-5}	0.9	4.4×10^{7}
3	7.8×10^{-10}	0.9	1.5×10^{5}	900	1.2×10^{-5}	0.9	3970	6.8×10^{-8}	0.9	2.2×10^{-5}	0.9	2.5×10^{7}
7	6.1×10^{-10}	0.9	3.6×10^{5}	7400	8.0×10^{-6}	0.9	7890	2.9×10^{-7}	0.9	2.1×10^{-5}	0.9	1.1×10^{7}
14	4.5×10^{-10}	0.9	5.9×10^{5}	7.4×10^{4}	6.0×10^{-6}	0.9	6.9×10^{4}	4.9×10^{-7}	0.9	1.7×10^{-5}	0.9	2.6×10^{6}
21	4.1×10^{-10}	0.9	1.6×10^{5}	1.5×10^{5}	2.5×10^{-6}	0.9	1.9×10^{5}	1.4×10^{-7}	0.9	7.4×10^{-6}	0.9	2.4×10^{6}
28	3.3×10^{-10}	0.9	2.1×10^{5}	2.2×10^{5}	1.9×10^{-6}	0.9	2.6×10^{5}	1.1×10^{-7}	0.9	7.5×10^{-6}	0.9	4.2×10^{6}
49	3.4×10^{-10}	0.9	3.5×10^{5}	5.8×10^{5}	1.1×10^{-6}	0.9	6.3×10^{5}	1.1×10^{-7}	0.9	7.4×10^{-6}	0.9	6.6×10^{6}
77	3.2×10^{-10}	0.9	6.0×10^{5}	1.5×10^{6}	7.7×10^{-7}	0.9	2.0×10^{6}	9.2×10^{-8}	0.9	7.9×10^{-6}	0.9	8.4×10^{6}
98	3.0×10^{-10}	0.9	8.9×10^{5}	2.5×10^{6}	4.6×10^{-7}	0.9	4.9×10^{6}	1.2×10^{-8}	0.9	7.5×10^{-6}	0.9	9.0×10^{6}
135	2.9×10^{-10}	0.9	1.8×10^{6}	5.7×10^{6}	3.7×10^{-7}	0.9	1.2×10^{7}	1.3×10^{-8}	0.9	7.6×10^{-6}	0.9	2.2×10^{7}

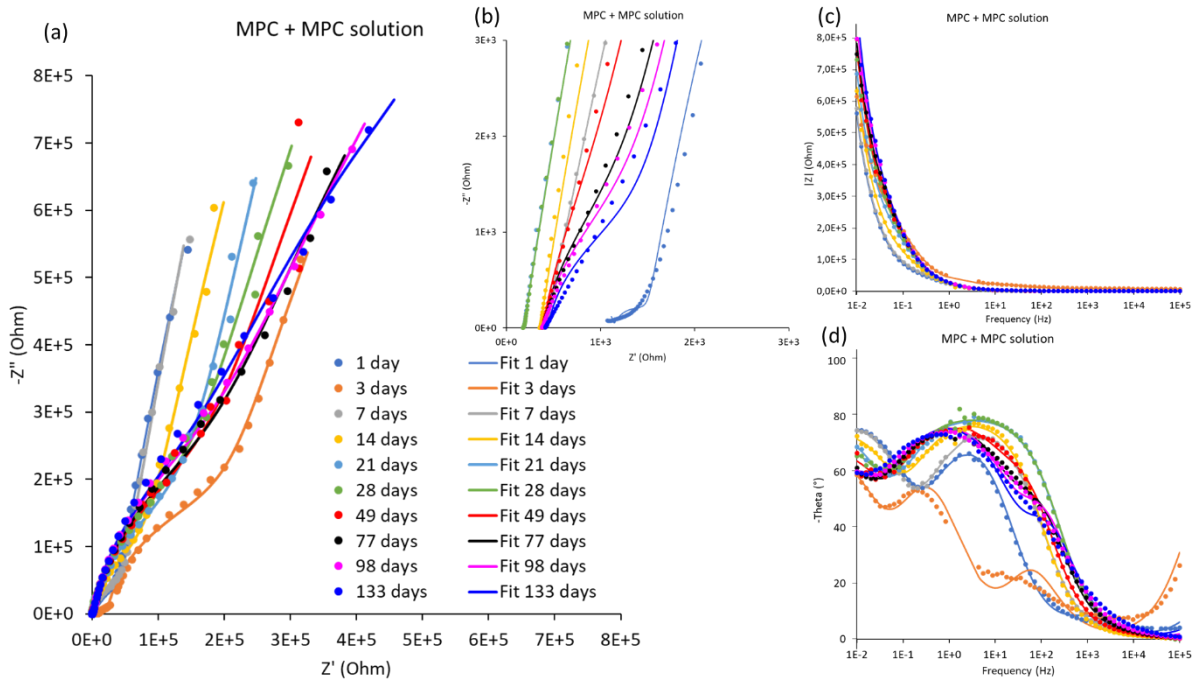

Figure 27. (a and b) Evolution of the Nyquist spectra and (c and d) evolution of the Bode spectra of beryllium in MPC mortar immersed in MPC solution in function of time (dots: experimental results; lines: fit).

Table 15. Fitting data of the EIS spectra of beryllium in MPC mortar immersed in MPC solution.

Days	CPE_m		R_{cp} (Ω)	R_{ncp1} (Ω)	CPE_{ncp1}		R_{ncp2} (Ω)	CPE_{ncp2}		CPE_{dl}		R_t (Ω)
	K_m ($F \cdot S^{\alpha}$)	α_m			K_{ncp1} ($F \cdot S^{\alpha}$)	$\alpha_{nc\ p1}$		K_{ncp2} ($F \cdot S^{\alpha}$)	$\alpha_{nc\ p2}$	K_{dl} ($F \cdot S^{\alpha}$)	α_{dl}	
1	5.6×10^{-10}	0.9	3.6×10^{4}	1565	1.1×10^{-5}	0.9	4868	6.0×10^{-8}	0.9	2.2×10^{-5}	0.9	1.8×10^{7}
3	4.5×10^{-10}	0.9	2.1×10^{5}	27605	6.5×10^{-6}	0.9	14445	1.9×10^{-7}	0.9	2.2×10^{-5}	0.9	6.2×10^{6}
7	2.8×10^{-10}	0.9	4.3×10^{4}	1770	4.6×10^{-6}	0.9	549	6.3×10^{-6}	0.9	2.2×10^{-5}	0.9	3.1×10^{7}
14	1.6×10^{-10}	0.9	7.8×10^{4}	380	1.3×10^{-5}	0.9	6193	8.0×10^{-7}	0.9	1.9×10^{-5}	0.9	1.4×10^{7}
21	4.5×10^{-10}	0.9	1.3×10^{5}	200	1.1×10^{-5}	0.9	2105	1.1×10^{-6}	0.9	1.9×10^{-6}	0.9	2.3×10^{7}
28	4.1×10^{-10}	0.9	1.5×10^{5}	200	1.1×10^{-5}	0.9	2009	1.1×10^{-6}	0.9	1.7×10^{-6}	0.9	9.3×10^{6}
49	2.9×10^{-10}	0.9	1.8×10^{5}	430	6.5×10^{-6}	0.9	3945	5.3×10^{-6}	0.9	1.8×10^{-6}	0.9	7.9×10^{6}
77	3.7×10^{-10}	0.9	2.0×10^{5}	470	3.6×10^{-6}	0.9	2490	8.2×10^{-6}	0.9	1.7×10^{-6}	0.9	4.9×10^{6}
98	4.6×10^{-10}	0.9	2.1×10^{5}	480	2.9×10^{-6}	0.9	2273	9.2×10^{-6}	0.9	1.6×10^{-6}	0.9	4.7×10^{6}
135	7.5×10^{-10}	0.9	1.7×10^{6}	575	2.0×10^{-6}	0.9	1944	1.2×10^{-5}	0.9	1.4×10^{-6}	0.9	3.4×10^{6}

Finally, to evaluate the effect of the low cost formulation of the MPC mortar on the corrosion of beryllium, some test were also realised in LC-MPC matrix containing no boric acid. The evolution of the Nyquist and Bode diagrams of beryllium metal exposed to LC-MPC mortar and to LC-MPC mortar immersed in MPC solution in function of time are shown in Figure 28 and Figure 29, respectively. The fitting values, using the EEC described in Figure 1d, are given in Table 16 and Table 17, respectively. Note that only the tests performed until 28 days are presented in this report but the experiments are continuing after the PREDIS project and will be the subject of a later publication.

Compared to the tests in MPC, tests in LC-MPC presented some similarities. For instance, the impedance corresponding to the MPC mortar (high to medium frequencies) increased with time, even if this increase was less pronounced (Figure 28c). The Nyquist plots showed a capacitive effect at lower frequencies (Figure 28a), corresponding to the passivation of the beryllium electrode, leading to similar R_t values as for the tests performed in MPC mortar (10^6-10^7 Ω; Table 16). However, until 28 days, no noise appeared in the EIS spectra, as observed during tests performed in MPC mortar. Note that it is important to recall that the LC-MPC mortar was not prepared in the glove box under argon atmosphere, like the other cement pastes and mortars. Samples were transferred to an argon atmosphere directly after hardening of the mortar (~1 hour after mixing). This could therefore induce some differences in the EIS data.

For the tests done in LC-MPC mortar immersed in MPC solution, triplicate tests gave different results. The obtained values of two extreme behaviours are represented in Figure 29 and Table 17. For one of the tests, R_t values were much lower, and therefore the corrosion rate was higher. One possible reason could be the presence of sodium thiosulphate that could trigger the corrosion of beryllium, as it was already observed for steel [29]. However, this test will need to be repeated in order to understand these different results.

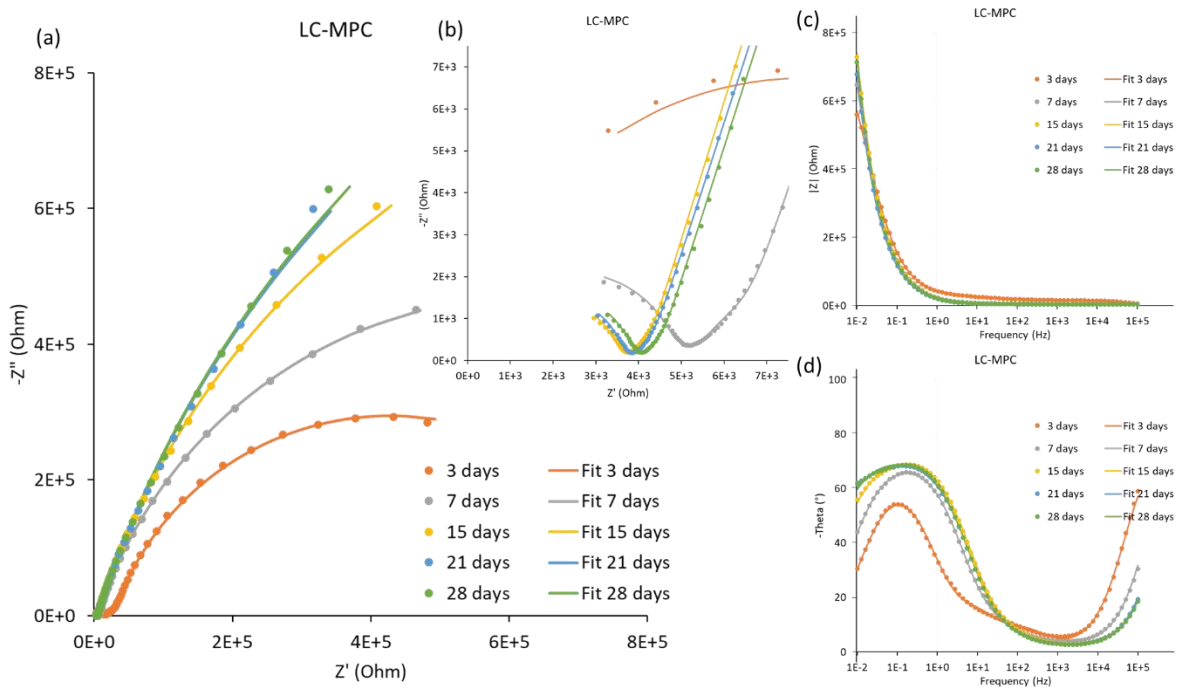

Figure 28. (a and b) Evolution of the Nyquist spectra and (c and d) Bode spectra of beryllium in LC-MPC mortar in function of time (dots: experimental results; lines: fit).

Table 16. Fitting data of the EIS spectra of beryllium in LC-MPC mortar.

Days	CPE_m		R_{cp} (Ω)	R_{ncp1} (Ω)	CPE_{ncp1}		R_{ncp2} (Ω)	CPE_{ncp2}		CPE_{dl}		R_t (Ω)
	K_m ($F \cdot S^{\alpha}$)	α_m			K_{ncp1} ($F \cdot S^{\alpha}$)	α_{ncp1}		K_{ncp2} ($F \cdot S^{\alpha}$)	α_{ncp2}	K_{dl} ($F \cdot S^{\alpha}$)	α_{dl}	
1	6.4×10^{-10}	0.9	5780	13460	1.3×10^{-8}	0.9	9780	4.4×10^{-7}	0.9	2.7×10^{-6}	0.90	1.8×10^{7}
3	7.9×10^{-10}	0.9	27710	70920	2.3×10^{-8}	0.9	74980	2.4×10^{-7}	0.9	9.4×10^{-6}	0.81	6.2×10^{6}
7	8.5×10^{-10}	0.9	6320	52790	3.1×10^{-9}	0.9	38130	9.8×10^{-8}	0.9	1.1×10^{-5}	0.81	3.1×10^{7}
15	6.4×10^{-10}	0.9	4150	56060	1.0×10^{-9}	0.9	43450	3.7×10^{-8}	0.9	1.1×10^{-5}	0.82	1.4×10^{7}
21	6.3×10^{-10}	0.9	4210	59810	1.4×10^{-9}	0.9	56400	3.4×10^{-8}	0.9	1.2×10^{-5}	0.81	2.3×10^{7}
28	5.6×10^{-10}	0.9	4420	71090	7.8×10^{-10}	0.9	56660	2.6×10^{-8}	0.9	1.2×10^{-5}	0.81	3.4×10^{6}

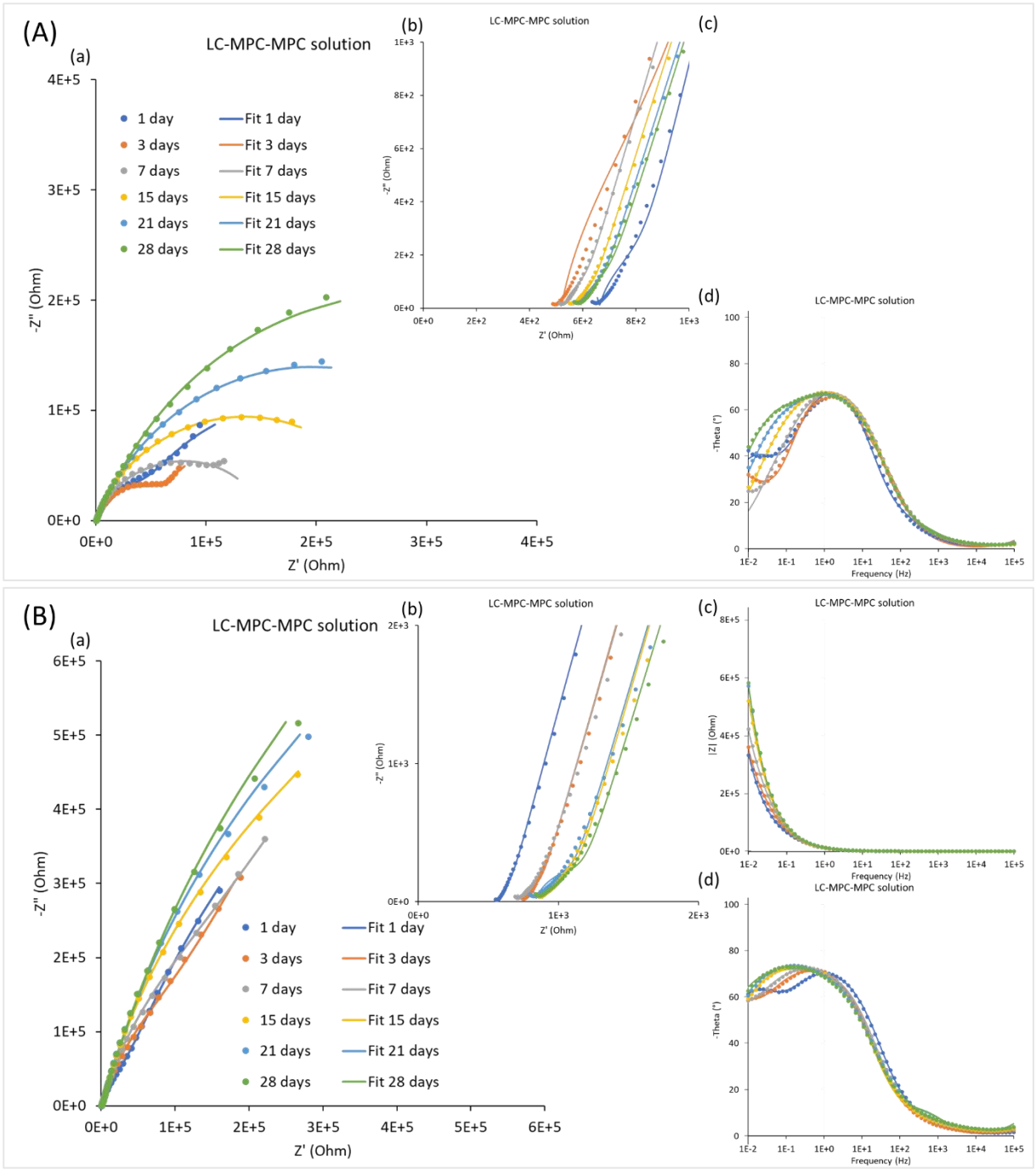

Figure 29. (a and b) Evolution of the Nyquist spectra and (c and d) Bode spectra of beryllium in LC-MPC mortar immersed in MPC solution in function of time (dots: experimental results; lines: fit). (A) and (B) represent different tests with extreme behaviour.

Table 17. Fitting data of the EIS spectra of beryllium in LC-MPC mortar immersed in MPC solution. Test (a) and Test (b) corresponds to extreme behaviour (see Figure 29).

Test	Days	CPE_m		R_{cp} (Ω)	R_{ncp1} (Ω)	CPE_{ncp1}		R_{ncp2} (Ω)	CPE_{ncp2}		CPE_{dl}		R_t (Ω)
		K_m ($F \cdot S^{\alpha}$)	α_m			K_{ncp1} ($F \cdot S^{\alpha}$)	α_{ncp1}		K_{ncp2} ($F \cdot S^{\alpha}$)	α_{ncp2}	K_{dl} ($F \cdot S^{\alpha}$)	α_{dl}	
(A)	1	6.9×10^{-10}	0.9	10840	780	1.1×10^{-5}	0.9	2370	3.1×10^{-5}	0.9	7.1×10^{-5}	0.9	1.8×10^{5}
	3*	1.0×10^{-10}	0.9	18890	560	3.8×10^{-7}	0.9	7210	8.4×10^{-7}	0.9	6.4×10^{-6}	0.7	1.2×10^{5}
	7	1.1×10^{-9}	0.9	2490	1720	1.2×10^{-6}	0.9	950	1.5×10^{-7}	0.9	1.4×10^{-5}	0.7	9.5×10^{4}
	15	8.9×10^{-10}	0.9	3530	800	3.9×10^{-5}	0.9	2280	1.1×10^{-6}	0.9	7.6×10^{-5}	0.7	9.7×10^{4}
	21	7.7×10^{-10}	0.9	2690	850	3.5×10^{-5}	0.9	2890	5.1×10^{-7}	0.9	7.0×10^{-5}	0.7	8.0×10^{4}
	28	6.8×10^{-10}	0.9	2020	910	2.9×10^{-5}	0.9	3440	2.5×10^{-7}	0.9	6.6×10^{-5}	0.7	6.4×10^{4}
(B)	1	4.3×10^{-10}	0.9	23460	5120	1.5×10^{-7}	0.9	660	5.0×10^{-5}	0.9	2.8×10^{-5}	0.82	2.1×10^{6}
	3	4.5×10^{-10}	0.9	80080	6700	1.0×10^{-7}	0.9	860	5.3×10^{-5}	0.9	3.0×10^{-5}	0.8	4.4×10^{6}
	7	6.1×10^{-10}	0.9	122690	4640	1.2×10^{-7}	0.9	860	5.3×10^{-5}	0.9	2.6×10^{-5}	0.8	4.2×10^{6}
	14	5.4×10^{-10}	0.9	311530	4720	1.4×10^{-7}	0.9	1090	5.2×10^{-5}	0.9	2.4×10^{-5}	0.8	2.9×10^{6}
	21	6.7×10^{-10}	0.9	478610	3920	1.6×10^{-7}	0.9	1070	5.4×10^{-5}	0.9	2.3×10^{-5}	0.8	2.6×10^{6}
	28	6.4×10^{-10}	0.9	450050	3880	1.6×10^{-7}	0.9	1150	6.8×10^{-5}	0.9	2.1×10^{-5}	0.8	3.6×10^{6}

*Presence of a Warburg element to allow a good fitting: W_s-R = 3.1×10^{6} Ω; W_s-T = 6900 s; W_s-P = 0.5

3.2.1.2 Corrosion rate calculation

As already presented in Section 3.1.2.2 for tests in solution, the corrosion rate of beryllium in cementitious matrices was calculated using the R_t values obtained from the fitting of the EIS data, and Equations 4 to 6. The evolution of the corrosion rate with time is presented in Figure 30 and Figure 31, and in Table 18 to Table 20.

Figure 30 shows that beryllium corroded faster in OPC paste than in MPC mortar. Even if both corrosion rates in cement paste/mortar were much lower than the ones measured in solutions, this reveals an opposite behaviour compared to the tests made in OPC and MPC solutions.

At the beginning of the test, the corrosion rate of beryllium in OPC paste immersed in OPC solution was higher (~1.2 µm/y after 3 days) than the rate in OPC paste (~0.5 µm/y after 3 days). This difference could be due to the higher availability of water in the system immersed in solution. However, already after 7 days, the corrosion rates measured in both conditions became comparable and remained so until the end of the test. After 140 days, the corrosion rate decreased to approximately (or even below) 0.1 µm/y. In MPC mortar, the corrosion rate was very low over the entire testing period and the corrosion rate never exceeded 0.05 µm/y. Note that the rate measured in MPC mortar immersed in MPC solution was lower (<0.01 µm/y) than the ones in MPC mortar. However, the uncertainty on these measurements was relatively high, due to the presence of noise in the recorded EIS curves.

Figure 31 shows the comparison of the evolution of the corrosion rate in MPC and LC-MPC mortars. At the beginning of the test, the corrosion rate recorded in LC-MPC mortar was higher than the one measured in MPC mortar. This can be due to the presence of thiosulfate that could increase the corrosion rate of beryllium, as this was reported for steel [29] or due to the presence of oxygen, as LC-MPC mortars were prepared in air, and not in the glove box under argon atmosphere as for the MPC mortars. However, more tests are needed to prove these hypotheses. Nevertheless, after 14 days, the corrosion rates of beryllium in MPC and in LC-MPC mortars were similar.

As mentioned in the previous section, results recorded from the beryllium samples embedded in the LC-MPC mortar immersed in MPC solution were not reproducible: the corrosion rate was as high as 1.8 µm/y after 28 days for one of the triplicate, which is the highest corrosion rate recorded when beryllium is embedded in cement paste or in mortar, while another one gave corrosion rates similar

to the one of the MPC samples (< 0.1 µm/y). Extra tests are therefore needed to better understand the results.

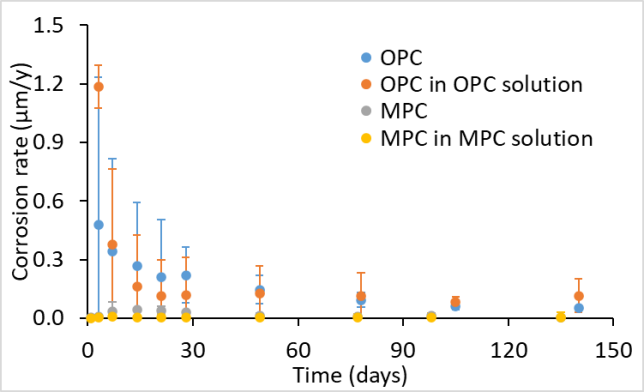

Figure 30. Comparison of the evolution of the corrosion rate of beryllium with time in OPC and MPC.

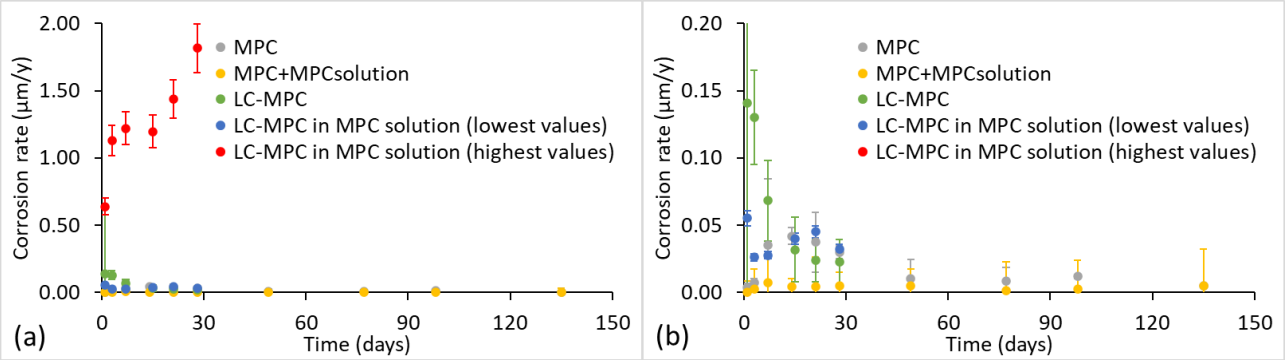

Figure 31. Comparison of the evolution of the corrosion rate of beryllium with time in MPC and LC-MPC. (b) is a zoom of (a) to allow a distinction between different systems.

Table 18. Average charge transfer resistance and corrosion rate of beryllium in OPC and OPC immersed in OPC solution.

OPC			OPC in OPC solution		
Days	R_t (Ω)	Corrosion rate (µm/y)	Days	R_t (Ω)	Corrosion rate (µm/y)
3	$(2.4 \pm 3.1)\times10^5$	0.48 ± 1.0	3	$(9.8 \pm 0.9)\times10^4$	1.19 ± 0.11
7	$(3.4 \pm 3.2)\times10^5$	0.34 ± 0.75	7	$(3.1 \pm 2.4)\times10^5$	0.37 ± 0.39
14	$(4.3 \pm 4.1)\times10^5$	0.27 ± 0.47	14	$(7.2 \pm 6.3)\times10^5$	0.16 ± 0.27
21	$(5.5 \pm 4.7)\times10^5$	0.21 ± 0.32	21	$(1.0 \pm 0.9)\times10^6$	0.11 ± 0.19
28	$(5.2 \pm 4.1)\times10^5$	0.22 ± 0.29	28	$(9.8 \pm 8.3)\times10^5$	0.12 ± 0.19
49	$(8.0 \pm 5.9)\times10^5$	0.14 ± 0.14	49	$(9.1 \pm 8.9)\times10^5$	0.13 ± 0.13
78	$(1.3 \pm 1.1)\times10^6$	0.09 ± 0.07	78	$(1.0 \pm 0.9)\times10^6$	0.11 ± 0.12
105	$(1.9 \pm 1.3)\times10^5$	0.06 ± 0.04	105	$(1.4 \pm 0.5)\times10^5$	0.08 ± 0.03
140	$(2.3 \pm 0.7)\times10^6$	0.05 ± 0.02	140	$(1.0 \pm 0.8)\times10^6$	0.11 ± 0.08

Table 19. Average charge transfer resistance and corrosion rate of beryllium in MPC and MPC immersed in MPC solution.

MPC			MPC in MPC solution		
Days	R_t (Ω)	Corrosion rate (µm/y)	Days	R_t (Ω)	Corrosion rate (µm/y)
1	$(3.3 \pm 3.1) \times 10^7$	0.004 ± 0.002	1	$(2.5 \pm 6.8) \times 10^8$	0.0005 ± 0.008
3	$(2.0 \pm 1.8) \times 10^7$	0.008 ± 0.003	3	$(4.0 \pm 9.1) \times 10^7$	0.003 ± 0.014
7	$(6.3 \pm 7.1) \times 10^6$	0.035 ± 0.049	7	$(1.5 \pm 2.2) \times 10^7$	0.008 ± 0.017
14	$(2.8 \pm 2.4) \times 10^6$	0.042 ± 0.006	14	$(2.6 \pm 3.4) \times 10^7$	0.004 ± 0.006
21	$(3.4 \pm 3.1) \times 10^6$	0.037 ± 0.022	21	$(2.6 \pm 3.7) \times 10^7$	0.004 ± 0.022
28	$(3.9 \pm 3.4) \times 10^6$	0.030 ± 0.005	28	$(2.3 \pm 3.9) \times 10^7$	0.005 ± 0.010
49	$(2.0 \pm 2.2) \times 10^7$	0.010 ± 0.014	49	$(2.2 \pm 4.0) \times 10^7$	0.005 ± 0.012
77	$(2.0 \pm 2.1) \times 10^7$	0.009 ± 0.010	77	$(6.7 \pm 11.8) \times 10^7$	0.002 ± 0.021
98	$(9.6 \pm 8.3) \times 10^6$	0.012 ± 0.002	98	$(4.7 \pm 6.7) \times 10^7$	0.002 ± 0.021
135	$(2.2 \pm 2.0) \times 10^7$	0.005 ± 0.004	135	$(2.2 \pm 4.0) \times 10^7$	0.005 ± 0.027

Table 20. Average charge transfer resistance and corrosion rate of beryllium in LCPC and LC-MPC immersed in MPC solution.

LC-MPC			LC-MPC in MPC solution		
Days	R_t (Ω)	Corrosion rate (µm/y)	Days	R_t (Ω)	Corrosion rate (µm/y)
1	$(8.2 \pm 15.9) \times 10^5$	0.141 ± 0.500	1	$(1.8 \pm 0.2) \times 10^5$	0.640 ± 0.064
				$(2.1 \pm 0.2) \times 10^6$	0.055 ± 0.006
3	$(8.9 \pm 2.6) \times 10^5$	0.130 ± 0.035	3	$(2.4 \pm 0.2) \times 10^5$	1.128 ± 0.113
				$(4.4 \pm 0.4) \times 10^6$	0.026 ± 0.003
7	$(1.7 \pm 0.7) \times 10^6$	0.068 ± 0.030	7	$(9.5 \pm 1.0) \times 10^4$	1.220 ± 0.122
				$(4.2 \pm 0.4) \times 10^6$	0.028 ± 0.003
14	$(3.6 \pm 2.1) \times 10^6$	0.032 ± 0.024	14	$(9.6 \pm 1.0) \times 10^4$	1.198 ± 0.120
				$(2.9 \pm 0.3) \times 10^6$	0.040 ± 0.004
21	$(4.8 \pm 2.5) \times 10^6$	0.024 ± 0.016	21	$(8.0 \pm 0.8) \times 10^4$	1.438 ± 0.144
				$(2.6 \pm 0.3) \times 10^6$	0.045 ± 0.005
28	$(5.0 \pm 2.7) \times 10^6$	0.023 ± 0.016	28	$(6.4 \pm 0.6) \times 10^4$	1.815 ± 0.182
				$(3.6 \pm 0.4) \times 10^6$	0.032 ± 0.003

* For LC-MPC in MPC solution, blue and red data correspond to extreme values (see blue and red markers in Figure 31).

3.2.2 Hydrogen measurement test

As explained in Section 2.2.2.2, the hydrogen measurement tests were divided in three main periods:

- 24 hours after the production, the cementitious materials containing the beryllium were demoulded and put into the container above water. This allow the curing of the cement paste/mortar in 100% RH condition;
- After 28 days, the containers were opened to remove the water and to create a dry atmosphere;
- Finally, after around 6 weeks in dry condition, the samples were immersed in the solution representative of the cement paste/mortar to mimic the resaturation of the pore network of the cement paste/mortar after potential breach of the steel container in the disposal repository.

Figure 32 and Table 21 show the evolution of the hydrogen gas released (and the corresponding corrosion rate) during the corrosion of beryllium in OPC and MPC.
Initially, when the samples were in 100% RH condition, the evolution of the gas production was similar for samples embedded in OPC paste and in MPC mortar. During the first 7 days of testing, the corrosion rate reached 0.8-0.9 µm/y (~10 mL $H_2/m^2 \cdot d$) and decreased further to 0.3-0.4 µm/y (3-6 mL $H_2/m^2 \cdot d$) after 28 days. In the dry period (between 28 and ~70 days), the corrosion rate continued to decrease until 0.08 and 0.04 µm/y (1-2 mL $H_2/m^2 \cdot d$) for samples embedded in OPC paste and MPC mortar, respectively. However, the decrease was sharper if beryllium was embedded in OPC paste. Therefore, at the end of this second period, two times more hydrogen gas was produced by the corrosion of beryllium embedded in MPC mortar (0.40±0.06 L/m²) compared to beryllium embedded in OPC paste (0.21±0.03 L/m²). While the hydrogen concentration remained stable after the immersion of beryllium embedded in MPC mortar in MPC solution (slight increase up to ~0.2 µm/y (~2.7 mL $H_2/m^2 \cdot d$)), a huge increase of the hydrogen production was observed after immersing beryllium embedded in OPC paste in OPC solution, leading to an increase of the corrosion rate up to ~2.6 µm/y (~32 mL $H_2/m^2 \cdot d$), 14 days after immersion. Later on, the corrosion rate decreased again to reach ~0.4 µm/y (~5.5 mL $H_2/m^2 \cdot d$) at the end of the test. Therefore, the volume of hydrogen released by the beryllium embedded in OPC paste exceeded the one released by beryllium embedded in MPC mortar. At the end of the test (one year), the total volume of hydrogen released was 1.68±0.25 and 0.97±0.15 L/m² for beryllium embedded in OPC paste and in MPC mortar, respectively.
Finally, the thickness of corroded beryllium, based on the hydrogen formed during the test, was calculated (Table 21). After one year, ~0.6 µm and ~0.2 µm of beryllium was corroded in OPC paste and MPC mortar, respectively.

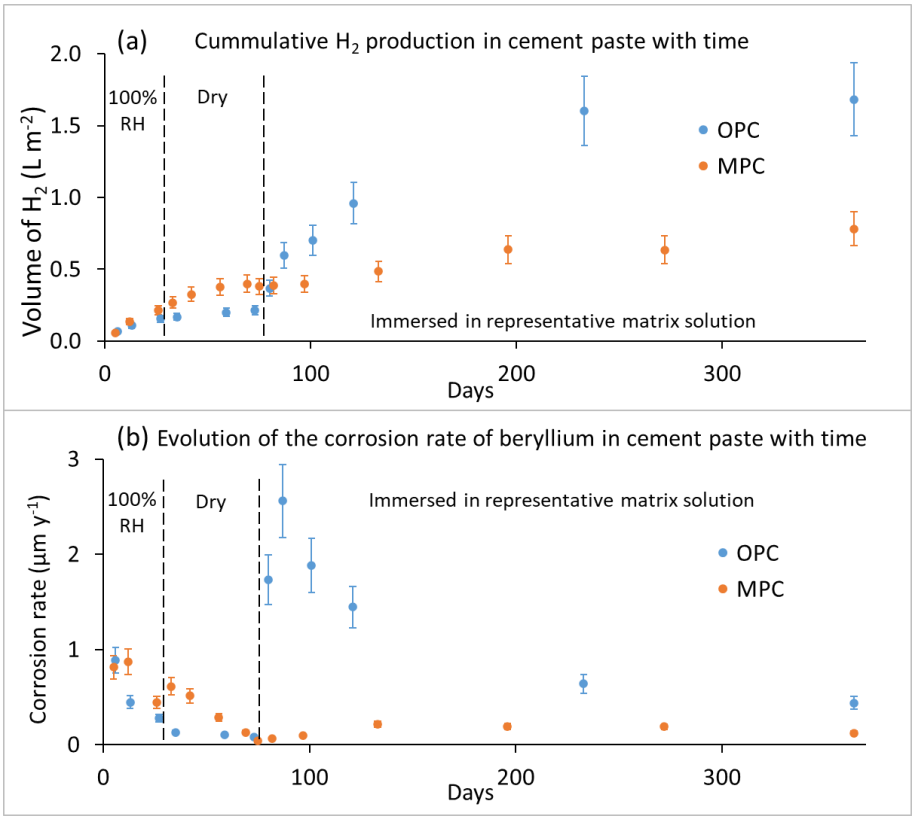

Figure 32. Leaching tests of beryllium pellets in OPC paste and MPC mortar. (a) Evolution of the cumulative volume of hydrogen produced and (b) the corresponding corrosion rate.

Table 21. Volume of hydrogen released, corresponding corrosion rate and calculated thickness of corroded beryllium in OPC paste and MPC mortar.

OPC paste					MPC mortar				
Days	Cumulative VH_2 production (L/m^2)	VH_2 between two sampling ($L/m^2 \cdot d$)	Calculated corrosion rate (µm/y)	Cumulative thickness of corroded Be (µm)	Days	Cumulative VH_2 production (L/m^2)	VH_2 between two sampling ($L/m^2 \cdot d$)	Calculated corrosion rate (µm/y)	Cumulative thickness of corroded Be (µm)
6	0.07	1.1×10^{-2}	0.89	0.015	5	0.06	1.0×10^{-2}	0.81	0.011
13	0.11	5.6×10^{-3}	0.45	0.023	12	0.14	1.1×10^{-2}	0.87	0.028
27	0.16	3.5×10^{-3}	0.28	0.034	26	0.21	5.6×10^{-3}	0.44	0.045
35	0.17	1.7×10^{-3}	0.13	0.037	33	0.27	7.7×10^{-3}	0.61	0.057
-	-	-	-	-	42	0.33	6.5×10^{-3}	0.51	0.069
59	0.20	1.3×10^{-3}	0.11	0.044	56	0.38	3.6×10^{-3}	0.29	0.080
-	-	-	-	-	69	0.40	1.6×10^{-3}	0.13	0.085
73	0.21	1.0×10^{-3}	0.08	0.047	75	0.40	4.9×10^{-4}	0.04	0.086
80	0.37	2.2×10^{-2}	1.74	0.080	82	0.41	8.6×10^{-4}	0.07	0.087
87	0.59	3.2×10^{-2}	2.56	0.129	97	0.42	1.2×10^{-3}	0.09	0.091
101	0.70	2.4×10^{-2}	1.88	0.201	133	0.52	2.7×10^{-3}	0.22	0.112
121	0.96	1.8×10^{-2}	1.45	0.280	196	0.68	2.4×10^{-3}	0.19	0.145
233	1.60	8.1×10^{-3}	0.64	0.476	272	0.83	2.4×10^{-3}	0.19	0.185
364	1.68	5.5×10^{-3}	0.44	0.634	364	0.97	1.6×10^{-3}	0.12	0.216

3.2.3 Characterisation

At the end of the hydrogen measurement tests, the samples were cut to gain more information on the interface between the beryllium metal and the cementitious matrix.

Figure 33 shows the interface between the beryllium and the OPC paste. A crevice is present between the cement paste and the metal. This is probably due to the drying process of the sample during the preparation procedure, as part of the cement paste is still partly sticking onto the metal. Figure 33(a, c and d) show that no corrosion product layer could be observed at the interface beryllium/OPC. However, needle-like particles with a length of maximum 5 µm, formed during the corrosion of the metal, were present in the whole cement paste close to the surface of beryllium. Figure 33(b) shows that these particles are present up to a front line (dash line) at ~300 µm from the metal. Unfortunately, it was difficult to gain information on the elemental composition of these particles as EDX mainly detect the elements from the cement paste and beryllium could not be detected.

Figure 34 shows the interface between the beryllium and the MPC mortar. From Figure 34 (a and b), no corrosion product were observed, which is coherent with the very little alteration expected from the hydrogen release tests. However, at some place in small amounts, needle-like particles could be observed close to the interface beryllium/MPC (arrow in Figure 34 c and d). However, there is no evidence that these particles result from the corrosion of beryllium.

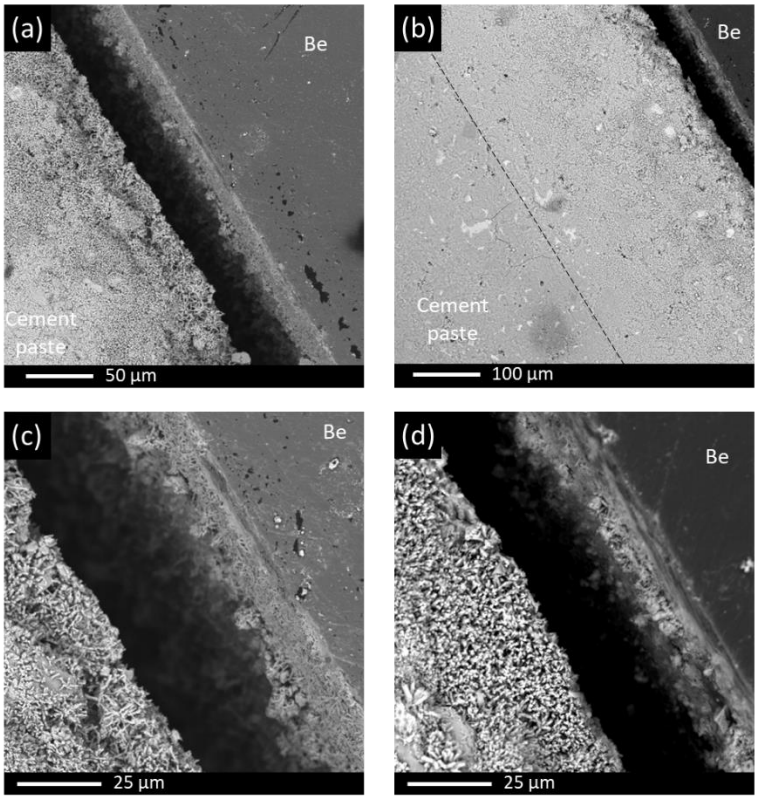

Figure 33. SEM micrographs of the interface between beryllium and OPC paste after the hydrogen measurement test.

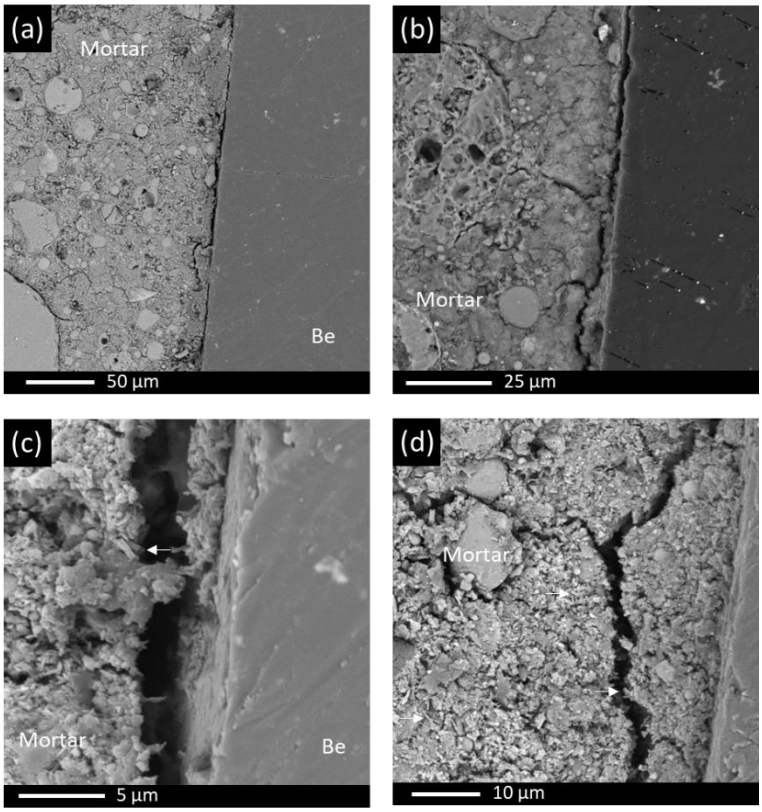

Figure 34. SEM micrographs of the interface between beryllium and MPC mortar after the hydrogen measurement test.

4 Conclusions

Due to its physical properties, beryllium is an attractive engineering material for nuclear applications, e.g. as moderator, reflector, or fuel cladding in thermal reactors. However, after irradiation, beryllium become brittle and beryllium wastes need to be disposed of. One option for the treatment and conditioning of the beryllium waste could be the direct emplacement of pieces of beryllium in a cementitious matrix.

The literature on the behaviour of beryllium in cementitious media is scarce and more studies are needed to fill the gaps. In this report, within the frame of the collaborative EC-funded Horizon 2020 project PREDIS, the corrosion behaviour of beryllium was studied in low-pH magnesium phosphate cement (MPC), in ordinary Portland cement (OPC), as well as in the representative cementitious pore solutions. To do so, many techniques were used to determine the corrosion rate of beryllium and to characterise the metal before and after corrosion, such as the mass loss determination, measurement of hydrogen produced during anaerobic corrosion of beryllium, analysis of the beryllium concentration in solution by ICP-MS, EIS, SEM and XRD. Two different beryllium grades were also evaluated in this study, e.g. pure beryllium and S-200-F grade beryllium.

The main findings of the study are the following:

- In high pH solutions (OPC solution and NaOH solution), similar corrosion behaviour was observed for both metal grade, whatever the technique used to determine the corrosion rate. From pH 12.5 to pH 14, the corrosion rate increase exponentially with pH. At pH ~13.5, the corrosion rate reached ~5 µm/y after 30 days of immersion and ~2 µm/y after 120 to 365 days of immersion. Moreover, the surface of both beryllium metal grade revealed pitting corrosion and a thin corrosion product layer. Mechanical defects (cavities, edges of scratches) on the initial beryllium surface acted as the initiation places for pitting corrosion.
- In near neutral pH solutions (MPC solution, with or without H_3BO_3 and NaOH solution), pure beryllium seemed to corrode slower (0.04 to 1.4 µm/y) than the S-200-F grade (~12 µm/y). The addition of boric acid helps decreasing the corrosion rate of beryllium in solution at pH ~7.7. SEM analysis of the surface of the metal after corrosion revealed the presence of $KBePO_4 \cdot H_2O$ crystals at the surface of both metal grade after corrosion in MPC solution.
- When beryllium is embedded in cementitious materials, the corrosion rates were lower than the ones measured in solutions with values lower or equals to 0.1 µm/y for tests in OPC paste. This corrosion rate is even lower in MPC mortar and it never exceeded 0.05 µm/y for tests recorded by EIS. The comparison of the corrosion of beryllium embedded in MPC and LC-MPC was difficult as the results obtained in LC-MPC were not reproducible. Extra tests are therefore needed to better understand the results. SEM analysis confirmed the little corrosion rate as no corrosion product layer was observed at the interface beryllium metal/cementitious material after the hydrogen measurement tests. However, needle-like particles with a length of maximum 5 µm were observed in the OPC paste close to the surface of beryllium up to a front line at ~300 µm from the metal.

REFERENCES

[1] Naik, B.G., Sivasubramanian, N., 1994. Applications of Beryllium and its alloys. Mineral Processing and Extractive Metallurgy Review 13, 243-251.

[2] Kurosaki, K., Yamanaka, S. 2020. Neutron Reflector Materials (Be, hydrides). Comprehensive Nuclear Materials 2, 307-321.

[3] Longhurst, G.R., Tsuchiya, K., Dorn, C.H., Folkman, S.L., Fronk, T.H., Ishihara, M., Kawamura, H., Tranter, T.N., Rohe, R., Uchida, M., Vidal, E. 2011. Managing Beryllium in Nuclear Facility Applications. Nuclear Technology 176, 430-441.

[4] BR2 – Belgian Reactor 2. SCK CEN website. 2024. https://www.sckcen.be/en/infrastructure/br2-belgian-reactor-2.

[5] Federici, G., Doerner, R., Lorenzetto, P., Barabash, V. 2012. Beryllium as a Plasma Facing Material for Near-Term Fusion Devices. Comprehensive Nuclear Materials 4, 621-666.

[6] Nakamichi, M., Kim, J.-H., Nakamura, M.M., Shibayama, T., Dorn, C.K., Vladimir, C., Bachurin, D.V., Stihl, C., Vladimirov, P.V. 2020. Beryllium and its alloys as neutron multiplying materials. Comprehensive Nuclear Materials 6, 203-250.

[7] Park, J.S., Bonnin, X., Pitts, R. 2021. Assessment of ITER divertor performance during early operation phases. Nuclear Fusion 61, 016021.

[8] Grambow, B., Lǒpez-García, M., Olmeda, J., Grivé, M., Marty, N.C.M., Grangeon, S., Claret, F., Lange, S., Deissmann, G., Klinkenberg, M., Bosbach, D., Bucur, C., Florea, I., Dobrin, R., Isaacs, M., Read, D., Kittnerová, J., Drtinová, B., Vopálka, D., Çevirim-Papaioannou, N., Ait-Mouheb, N., Gaona, X., Altmaier, M., Nedyalkova, L., Lothenback, B., Tits, J., Landesman, C., Rasamimanana, S. & Ribet, S. 2020. Retention and diffusion of radioactive and toxic species on cementitious systems: Main outcome of the CEBAMA project. Applied Geochemistry 112, 104480.

[9] Hill, M.A., Buft, D.P., Litlard, R.S. 1998. The passivity and Breakdown of Beryllium in Aqueous Solutions. Journal of Electrochemical Society 145, 2799-2806.

[10] Cannes, C., Bouhier, P., Lambertin, D., Grisolia, C. 2023. Reactivity of beryllium in aqueous solution from acidic to basic pH. Journal of Electroanalytical Chemistry 950, 117879.

[11] Çevirim-Papaioannou, N., Gaona, X., Böttle, M., Yalçintaş Bethune, E., Schild, D., Adam, C., Sittel, T. & Altmaier, M. 2020. Thermodynamic description of Be(II)solubility and hydrolysis in acidic to hyperalkaline NaCl and KCl solutions. Applied Geochemistry 117, 104601.

[12] Pourbaix, M. 1963. Atlas D'équilibres Électrochimiques. Paris: Gauthier-Villars & Cie.

[13] Bouhier, P. 2022. Conditionnement des déchets nucléaires de béryllium : réactivité dans différentes matrices cimentaires et comparaison avec l'aluminium. PhD thesis. Université Paris-Saclay.

[14] Bouhier, P., Cannes, C., Lambertin, D., Grisolia, C., Rodrigues, D. & Delpech, S. 2022. Evaluation of several conditioning matrices for the management of radioactive metal beryllium wastes. Journal of Nuclear Materials, 559, 153464.

[15] Le, K.-K., Sayenko, S., Stefan, L. 2022. Low-cost magnesium phosphate cement (LC-MPC) formulations. Milestone MS29 of the PREDIS EC-project.

[16] S. Caes, A. Gurning, Li, X., De Souza, V., Kursten, B. 2023. Corrosion of aluminium in ordinary Portland cement paste: influence of matrix porosity and the presence of $LiNO_3$ corrosion inhibitor. Materials and Corrosion 74, 125-137.

[17] Delpech, S., Cannes, C., Barré, N., Tran, Q.T., Sanchez, C., Lahalle, H., Lambertin, D., Gauffinet, S., Cau-dit-Coumes, C. 2017. Kinetic Model of Aluminium Behavior in Cement-Based Matrices Analyzed by Impedance Spectroscopy. Journal of Electrochemical Society 164, C717.

[18] Çevirim-Papaioannou, N., Androniuk, I., Miron, G.D., Altmaier, M. & Gaona, X. 2023. Beryllium solubility and hydrolysis in dilute to concentrated CaCl2 solutions: thermodynamic description in cementitious systems. Frontiers in Nuclear Engineering 2, 1192463.

[19] Cau-dit-Coumes, C., Lambertin, D., Lahalle, H., Antonucci, P., Cannes, C., Delpech, S. 2014. Selection of a mineral binder with potentialities for the stabilization/solidification of aluminium metal. Journal of Nuclear Materials 453, 31-40.

[20] English, J.L. 1955. The metal beryllium. Cleveland: American Society for Metals.

[21] Prochko, R.J., Myers, J.R., Saxer, R.K. 1966. Material Protection 5, 39-42.

[22] Chatalov, A.Y. 1952. Dokl. Akad Nauk, SSSR 86, 775-777.

[23] Bukaemskiy, A., Caes, S., Modolo, G., Deissmann, G., Bosbach, D. 2024. Investigation of kinetics and mechanisms of metallic beryllium corrosion for the management of radioactive wastes. MRS Advances, https://doi.org/10.1557/s43580-024-00835-y.

[24] Wyckoff, R.W.G. 1963. Crystal Structures Vol. 1. New-York: Interscience Publishers.

[25] Stahl, R., Jung, C., Lutz, H.D., Kockelmann, W., Jacobs, H. 1998. Zeitschrift für Anorganische und Allgemeine Chemie 624, 1130-1136.

[26] West, J.M. 1970. Electrodeposition and corrosion processes. New-York: Interscience Publishers.

[27] Punni, J.S., Cox, M.J. 2010. The effect of impurity inclusions on the pitting corrosion behaviour of beryllium. Corrosion Science 52, 2535-2546.

[28] Lillard, R.S. 2001. Factors Influencing the Transition from Metastable to Stable Pitting in Single-Crystal Beryllium. Journal of the Electrochemical Society 148, B1-B11.

[29] Choudhary, L., Macdonald, D., Alfantazi, A. 2015. Role of thiosulfate in the corrosion of steels: a review. Corrosion 71, 150602132136005.

Annex 1 – Calculation of the beryllium corrosion rate from H_2 concentration measured by GC

H_2 concentration in the headspace of the container ($[H_2]$) = 328.93 µL/L

Volume of the headspace of the container (V_c) = 0.28344 L

Pressure of the container (P_c)= 3.049 bar

The volume of H2 in the container (at atmospheric pressure = pressure of the GC) is given by Equation A1:

$$V_{H2}(L) = \frac{[H_2]\times V_c \times P_c}{1\times 10^6} = 2.48 \times 10^{-4}\ L \qquad \text{(Equation A1)}$$

Knowing the density of H_2 (ρ_{H2} = 0.08988 g/L) and the molecular mass of H_2 (MM_{H2} = 2.01594 g/mol), the number of mole of H_2 (n_{H2}) produced can be calculated via Equation A2.

$$n_{H2}(mole) = \frac{\frac{\rho_{H2}}{V_{H2}}}{MM_{H2}} = 1.27 \times 10^{-5}\ mole \qquad \text{(Equation A2)}$$

Knowing that one mole of beryllium corroded produces one mole of hydrogen, the number of mole of beryllium corroded ($n_{Be,c}$) equals to the number of H_2 mole produced (Equation A3)

$$n_{Be,c} = n_{H2} \qquad \text{(Equation A3)}$$

Knowing the molecular mass of beryllium (MM_{Be} = 9.013 g/mol), the density of beryllium (ρ_{Be} = 1.85 g/cm³) and the surface area of beryllium in contact with the solution (SA_{Be} = 15.77 cm³ in this example), it is possible to calculate the thichness of beryllium corroded ($T_{Be,c}$) in the time period between two samplings/GC analysis (Equation A4).

$$T_{Be,c}\ (cm) = \frac{\frac{n_{Be,c}\times MM_{Be}}{\rho_{Be}}}{SA_{Be}} = 3.92 \times 10^{-6}\ cm \qquad \text{(Equation A4)}$$

Finally, knowing the time period between two samplings/GC analysis (Δt = 7 days in this example), it is possible to calculate the corrosion rate of beryllium (CR_{Be}) (Equation A5).

$$CR_{Be}\ (\mu m/y) = \frac{T_{Be,c}}{\Delta t} \times 365.25 \times 10^6 = 2.04\ \mu m/y \qquad \text{(Equation A5)}$$